electronics

Article

Hybrid Converter with Multiple Sources for Lithium Battery Charger Applications

Sheng-Yu Tseng *, Jun-Hao Fan and Hong-Kai Huang

Department of Electrical Engineering, Chang Gung University, Taoyuan 33302, Taiwan; m0921014@cgu.edu.tw (J.-H.F.); m0721111@cgu.edu.tw (H.-K.H.)
* Correspondence: sytseng@mail.cgu.edu.tw; Tel.: +886-3-211-8800 (ext.5706)

Abstract: This paper proposes a hybrid converter with multiple sources for lithium battery charger applications. Since the output voltage of a lithium battery charger is very low, its charger needs a higher step-down voltage for a utility line source or a step-down voltage for PV arrays. In order to implement the battery charger with utility line and PV arrays sources to simultaneously supply power to battery, a flyback converter is selected for utility line sources, and a buck converter is adopted for PV arrays source. Due to leakage inductor of transformer in flyback converter, an active clamp circuit is introduced into flyback converter to recover the energy stored in leakage inductor. In addition, flyback and buck converters can adopt switch integration techniques to simplify circuit structure. With this approach, the proposed hybrid converter has less components, is lighter weight and has smaller size and higher conversion efficiency. Finally, a prototype of the proposed hybrid converter with output voltage of 5 V~8.4 V and output maximum current of 12 A has been implement to verify its feasibility. It is suitable for the lithium battery charger applications.

Keywords: hybrid converter; lithium battery; charger; flyback converter; buck converter

check for updates

Citation: Tseng, S.-Y.; Fan, J.-H.; Huang, H.-K. Hybrid Converter with Multiple Sources for Lithium Battery Charger Applications. *Electronics* **2022**, *11*, 616. https://doi.org/10.3390/electronics11040616

Academic Editor: Jahangir Hossain

Received: 30 December 2021
Accepted: 14 February 2022
Published: 16 February 2022

1. Introduction

Currently, advances in switching power supply technology have created high energy density with lower volume, size and cost. It is widely applied to power systems to generate electric power to load, such as ac/dc converter, dc/dc converter, uninterrupted power supply (UPS), induction heating, electronic ballast, telecom power supplies, light emitting diode drivers and battery charger and dischargers [1–5]. In particular, battery power is rapidly replacing fossil fuel as an energy storage system in a variety of power system application, such as energy storage cabinet system, UPS, electric vehicle, small bikes, garden tools, vacuum cleaners and 3C products [6–10].

In general, battery power is combined with renewable energy sources to generate electric power to load due to zero pollution. In particular, when solar power is regarded as an input power source of power processor, different types of power sources should be merged to transfer less fluctuated and more reliable energy to load due to its intermittent feature. In order to supply power to the battery, a utility line source is selected to help solar power to sustain continuous energy to battery when solar power is functioning with less intense solar radiation. Therefore, solar power sources and utility line sources are simultaneously selected in the proposed power system to increase power reliability for battery charging applications.

When charger is widely used in power systems, various battery types are chosen to achieve storage energy. Since lithium battery possesses high energy density, small size and low self-discharge [11–13], it is extensively adopted in portable products. However, the lifetime of lithium battery is easily affected by the charging method. In order to increase life time of lithium battery, many battery charging methods have been proposed [14–16]. They include constant trickle current (CTC), constant current (CC) and constant current/constant voltage (CC-CV) charging methods. In these methods, since CTC charging method requires a longer charging time, its applications are limited. Since the CC-CV charging method can reduce charging time, it is suitable for the utility line source system. In addition, battery charger adopts solar power as it input source. To implement maximum power point tracking (MPPT) of solar power, the CC charging method can be used to extract its maximum power. Therefore, CC-CV and CC charging methods are, respectively, adopted in the proposed power system operated in the utility line and solar power source conditions.

In general, a battery cell is connected in series or parallel to form a battery pack for power system applications. Since a battery pack uses a lot of battery cells connected in series, it will result in voltage difference between each battery cell. Therefore, the lifetime and maximum storage capacity of battery pack can be reduced. In order to obtain better lifetime and maximum storage capacity of the battery, a battery pack with two or three battery cells connected in series is usually adopted without a battery equalizer. Its output voltage is less than 13 V. When a battery charger uses the utility line source as its input source, it needs a high step-down converter. Due to the low-level power application of the proposed charger, a flyback or forward converter can be selected as the charging converter. Moreover, a flyback converter has a better circuit and costs less. It is regarded as the charger when the proposed power system is operated in the utility line source condition, as shown in Figure 1. If the proposed one adopts solar power as its input source, a buck converter can be chosen as the charger because of low voltage differences between the output voltage of solar power and the battery, as shown in Figure 2. Therefore, the proposed power system operated in the utility line source condition adopts a flyback converter as its charger, while the proposed one operated in the solar power source condition uses a buck converter as its charger.

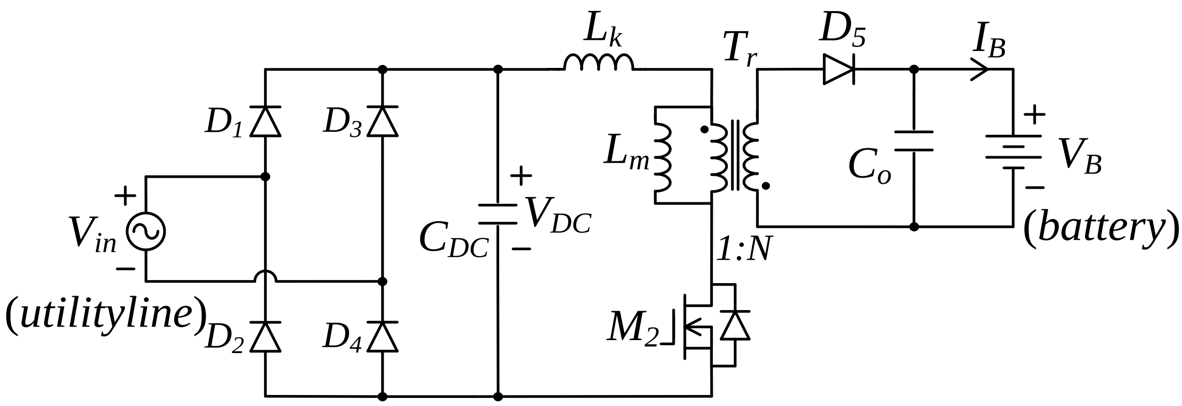

Figure 1. Schematic diagram of flyback converter for battery charging system.

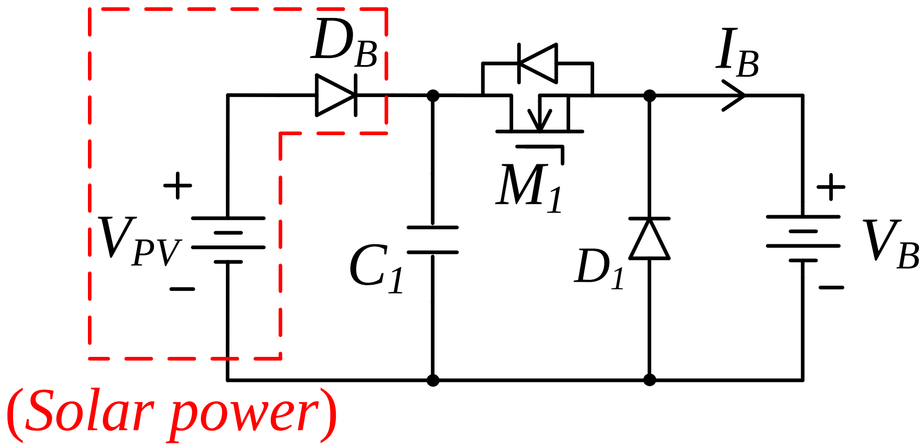

Figure 2. Schematic diagram of buck converter for battery charging system.

The proposed power system can select flyback and buck converters to achieve multiple sources for lithium battery charger applications, as shown in Figure 3. Since transformer T_r in flyback converter exists with leakage inductance L_K, it will induce a spike voltage across switch M_1 when switch M_1 is switched off. In order to recover the energy trapped in leakage inductance L_K, an active clamp circuit is introduced into the flyback converter to increase conversion efficiency [17–20]. Moreover, a buck converter can adopt a bidirectional circuit to implement the battery charger. For further simplifying circuit topology of the proposed power system, switches of active clamp flyback and bidirectional buck converters can be merged to form a hybrid converter, as shown in Figure 4. In Figure 4, since the utility line source and solar power source conditions are separately operated and their exchange time is very long, switch S_1 with a low speed and low cost is adopted to control operational conditions. In addition, the proposed hybrid converter can use less components and is of lighter volume, smaller size, lower cost and higher conversion efficiency. It is suitable for battery charger systems with multiple sources, such as Ni-Cd, Ni-MH, lead-acid, lithium batteries, etc.

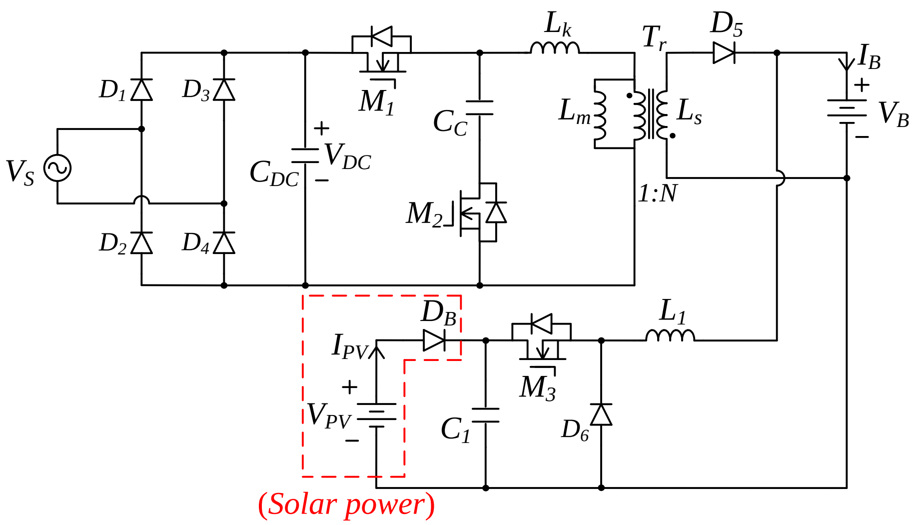

Figure 3. Schematic diagram of the conventional flyback/buck hybrid converter with utility line and PV arrays sources for lithium battery charger system.

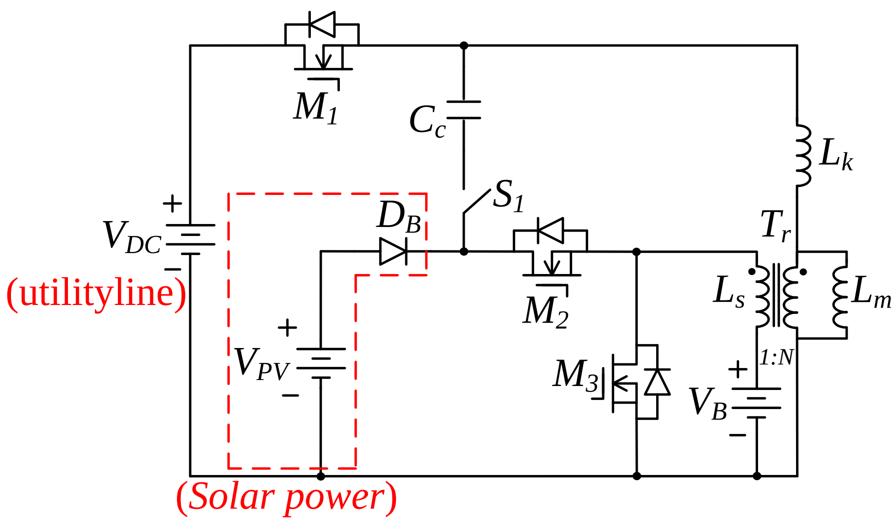

Figure 4. Schematic diagram of the proposed hybrid converter.

The multiport converter has been widely applied to generate electric power [21–26]. In [21], a multi-port converter was used in smart grid for the integration of storage and distributed generator. The authors of [22] proposed a multi-input dc-dc converter to transfer power from different power sources to the load. In order to implement input source of converter with multiple power sources, their component counts were added, and their driving circuits are complex. In [23–26], they are adopted in PV and battery system for supplying power to load. They possess dual input and single output ports. The proposed hybrid converter is shown in Figure 4. It is similar to three-port converter: dual inputs and single output. Comparison of component counts with the proposed hybrid converter and its counterparts is illustrated in Table 1. From Table 1, it can be observed that the proposed one can implement dual inputs and single output. It only uses one transformer, three switches, one capacitor and one extra switch. Compared with its counterparts, the proposed hybrid converter can reduce component counts to achieve approximately functions.

Table 1. Comparison of component counts with the proposed hybrid converter and its counterparts.

Three-Port Converter	Input Ports	Output Ports	Inductors	Transformers	Switches	Diodes	Capacitors	Extra Switches
M. Kumar, et al. [23]	2	1	2	0	3	3	3	0
H. Wu, et al. [24]	2	1	2	0	3	3	1	0
H. Wu, et al. [25]	2	1	3	0	3	3	1	0
Y-E. Wu, et al. [26]	2	1	1	1	4	2	3	0
The proposed Hybrid converter (Figure 4)	2	1	0	1	3	0	1	1

2. Derivation of the Proposed Hybrid Converter

Since the proposed hybrid converter includes an active clamp flyback and buck converter for battery charging applications, illustrated in Figure 3, it will become a complex circuit structure. In Figure 3, the active clamp flyback and buck converters are operated at different times, and the operational time of each converter is very long. Therefore, two sets of converters can be integrated as a hybrid converter. In the following, a circuit structure derivation is briefly described.

In order to simplify circuit structure of the proposed hybrid converter, diodes D_5 and D_6 shown in Figure 3 are, respectively, changed by switches M_{D5} and M_{D6} illustrated in Figure 5a. In Figure 5a, when switch M_{D5} is moved from the upper regions to the lower loop, which consists of switch M_{D5}, voltage V_B and inductor L_S, the operation of the proposed power system is not affected, as shown in Figure 5b. If switches M_{D5} and M_{D6} are operated synchronously, two switches can be merged by switch M_{D56}. Moreover, inductors L_1 and L_S can be integrated to form inductors L_{1S}, as shown in Figure 5c.

n order to further simplify the proposed power system, nodes A and A′ are regarded as the same node AA′. Its circuit structure is illustrated in Figure 5d. When the operational condition of the proposed one is operated in the flyback converter condition, switches M_2 and M_{D56} are switched on or switched off at the same time. Therefore, the S terminal of switch M_2 connected in node AA′ can be moved to node B. The operation of the proposed one is not affected, as shown in Figure 5e. Since flyback and buck converters are operated at different times and their exchange time is very long, switch S_1 with low speed and low cost can be used to control the operational condition of the proposed power system. Therefore, switches M_2 and M_3 are integrated to form switch M_{23}, as shown in Figure 5f. To simplify component symbol, the component devices of the proposed hybrid converter are renamed, as shown in Figure 4. From Figure 4, it can be observed that proposed hybrid converter can use less component counts to implement battery charger under utility line and solar power sources.

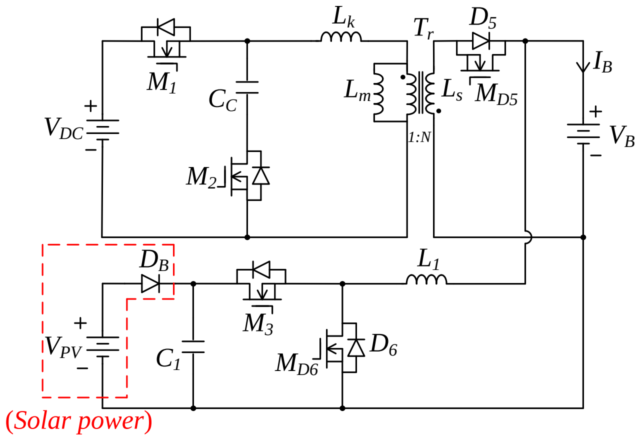

(**a**)

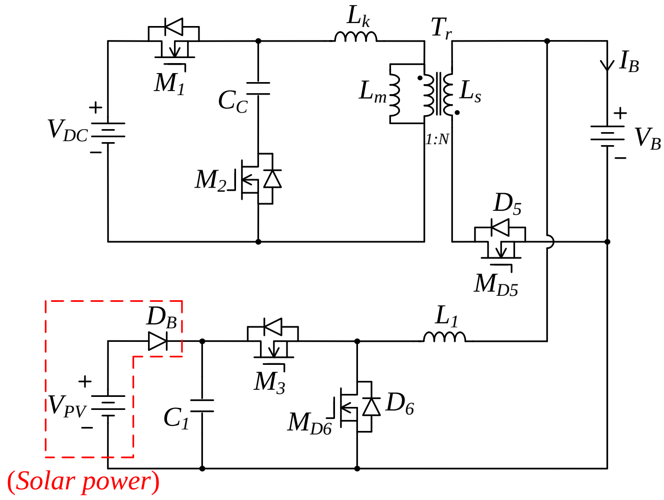

(**b**)

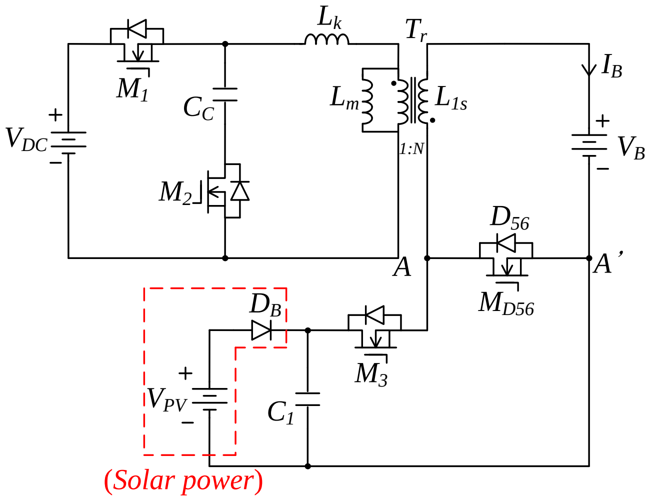

(**c**)

Figure 5. *Cont.*

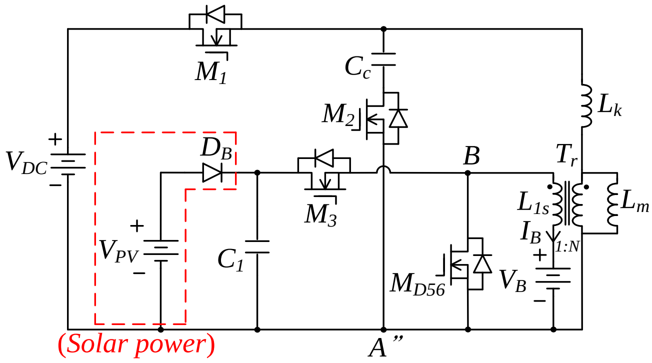

(**d**)

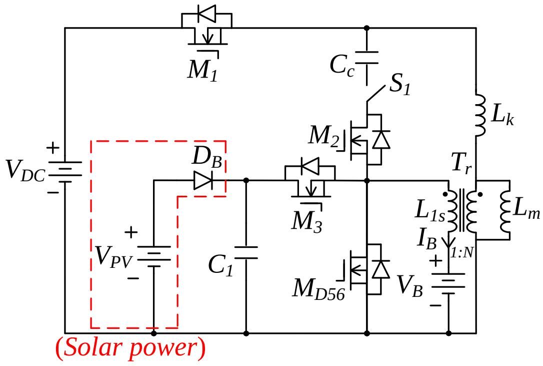

(**e**)

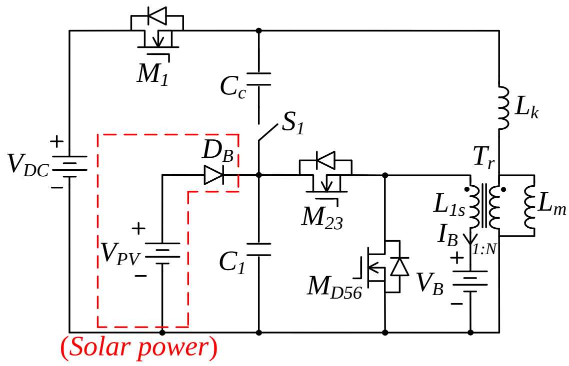

(**f**)

Figure 5. Circuit derivation of the proposed hybrid converter with utility line and PV arrays sources for lithium battery charger system: (**a**).step 1, (**b**) step 2, (**c**) step 3, (**d**) step 4, (**e**) step 5 and (**f**) step6.

In order to further simplify the proposed power system, nodes A and A′ are regarded as the same node AA′. Its circuit structure is illustrated in Figure 5d. When the operational condition of the proposed one is operated in the flyback converter condition, switches M_2 and M_{D56} are switched on or switched off at the same time. Therefore, the S terminal of switch M_2 connected in node AA′ can be moved to node B. The operation of the proposed one is not affected, as shown in Figure 5e. Since flyback and buck converters are operated at different times and their exchange time is very long, switch S_1 with low speed and low cost can be used to control the operational condition of the proposed power system. Therefore, switches M_2 and M_3 are integrated to form switch M_{23}, as shown in Figure 5f. To simplify component symbol, the component devices of the proposed hybrid converter are renamed, as shown in Figure 4. From Figure 4, it can be observed that proposed hybrid converter can use less component counts to implement battery charger under utility line and solar power sources.

3. Operational Principle of the Proposed Hybrid Converter

The proposed hybrid converter can be operated in the utility line source and solar power source conditions for lithium battery charging applications. When the proposed one is operated in the solar power source condition, its equivalent circuit is illustrated in Figure 6a by the blue line. Figure 6b shows equivalent circuit of the proposed one operated in the utility line source condition by the blue line. In order to explain the operational principle of the proposed one, each converter is briefly described in the following.

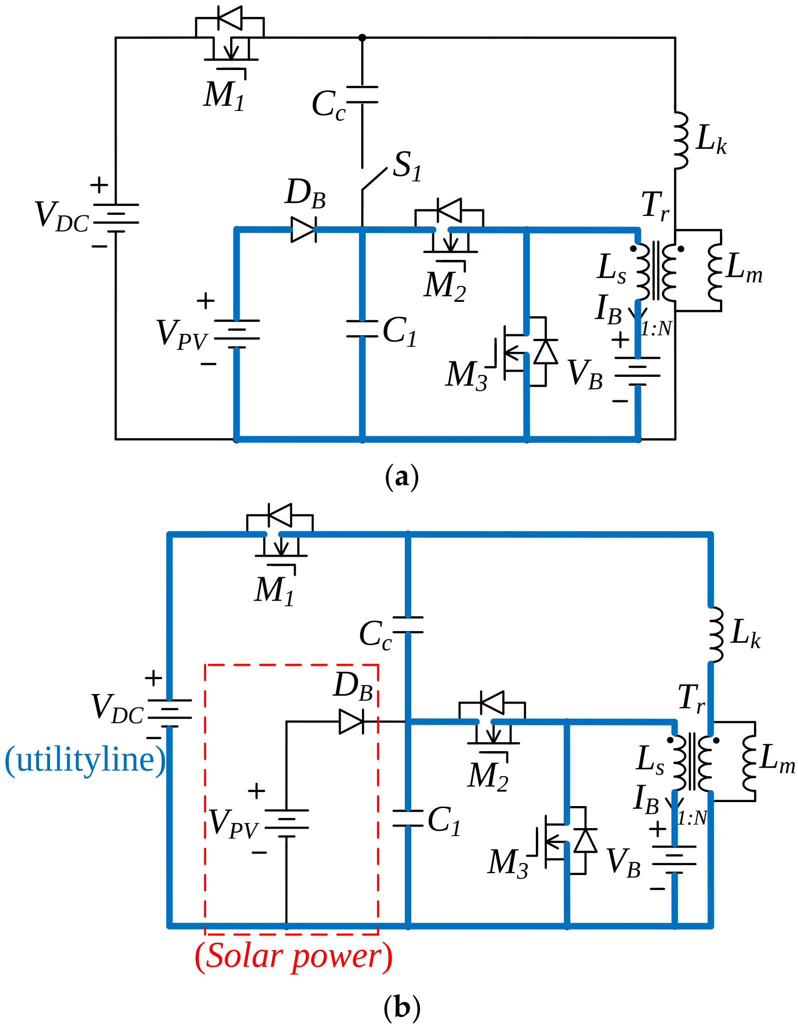

Figure 6. Equivalent circuit of the proposed hybrid converter in (**a**) buck converter mode for PV array source and (**b**) flyback converter mode for utility line source.

A. The solar power source condition: buck converter

When the proposed hybrid converter is operated in the solar power source condition, its equivalent circuit is shown in Figure 6a. Its equivalent circuit is a buck converter. Since the operational state of the proposed converter is always in continuous conduction mode (CCM) from light load to heavy load, its operational principle with CCM is briefly described. According to the operational principle of the proposed converter operated in the solar power source condition, its operational principle can be divided into five modes. Figure 7 illustrates an equivalent circuit of each operational mode by the blue line. While Figure 8 shows conceptual waveforms of each operational mode over a complete switching cycle. In the following, each operational mode is briefly explained.

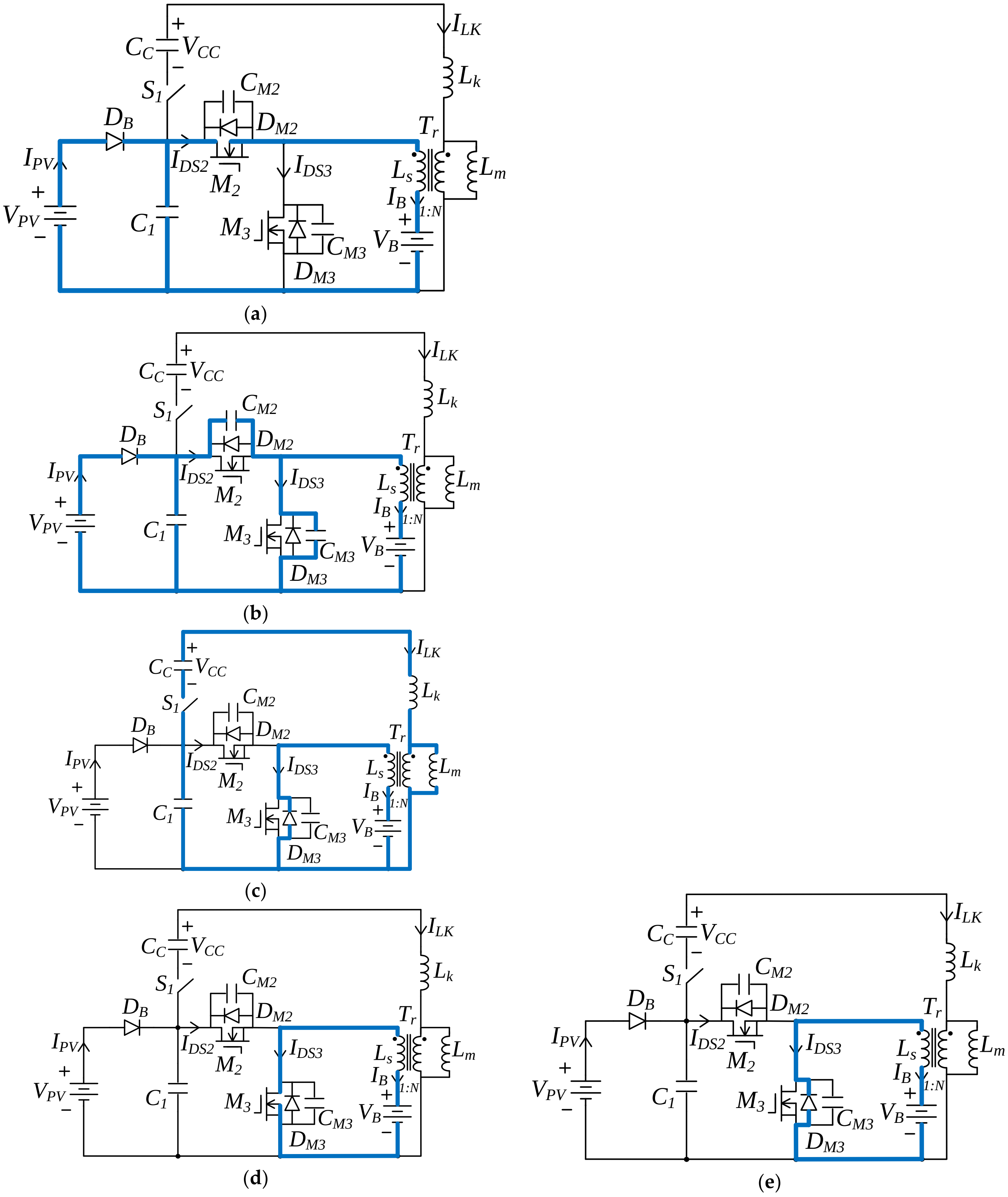

Figure 7. Equivalent circuit of each operational mode of the proposed hybrid converter operated in PV arrays source condition over a complete switching cycle. (**a**) Mode1 ($t_0 \leq t \leq t_1$), (**b**) Mode2 ($t_1 \leq t \leq t_2$), (**c**) Mode3 ($t_2 \leq t \leq t_3$), (**d**) Mode4 ($t_3 \leq t \leq t_4$) and (**e**) Mode5 ($t_4 \leq t \leq t_5$).

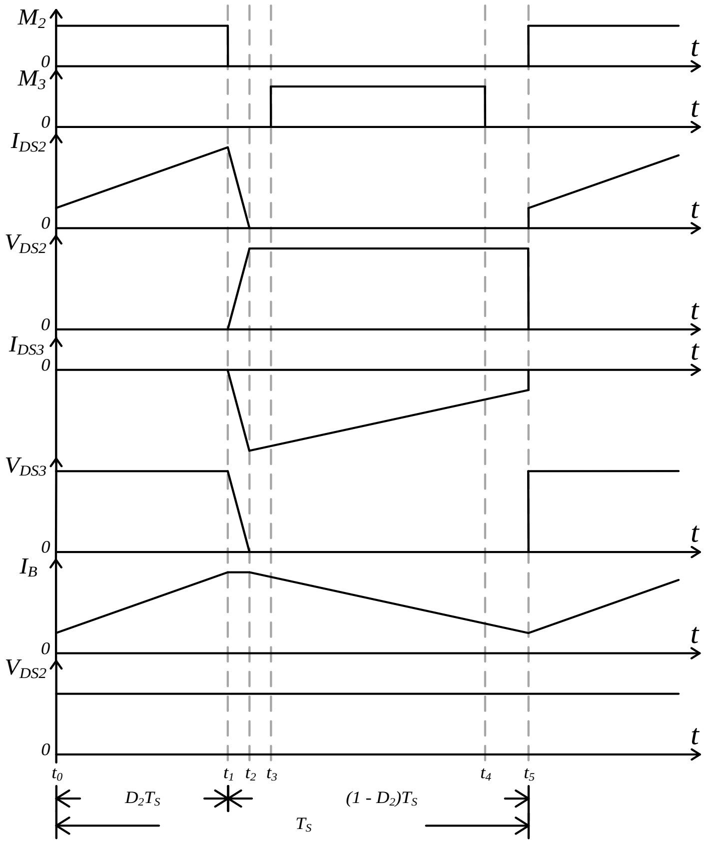

Figure 8. Conceptual waveforms of each operational mode of the proposed hybrid converter operated in the PV arrays source condition over a complete switching cycle.

Mode 1 (Figure 7a: $t_0 \leq t < t_1$): Before t_0, switches M_2 and M_3 are in the off state. Diode D_{M3} is in the forward bias state. When $t = t_0$, switch M_2 is switched on. Since switch current I_{DS3} is equal to ($-I_B$), switch current I_{DS2} abruptly increases from 0 A to I_B. Therefore, diode is D_{M3} reversely biased. During this time interval, current I_B linearly increases and inductor L_s is in the storage energy state.

Mode 2 (Figure 7b: $t_1 \leq t < t_2$): At t_1, switch M_2 is switched off and switch M_3 is kept in the off state. Within this time interval, since inductor current I_B has to be sustained at continuous state, capacitor C_{M2} is operated in the charging state, while C_{M3} is sustained in the discharging state. Therefore, voltage V_{DS2} varies from 0 V to V_{PV} and voltage V_{DS3} changes from V_{PV} to 0 V.

Mode 3 (Figure 7c: $t_2 \leq t < t_3$): When $t = t_2$, switches M_2 and M_3 are kept in the off state. At the moment, voltage V_{DS3} is equal to 0 V. Diode D_{M3} is forwardly biased. During this time period, inductor L_s is in the released energy state. Its current, I_B, linearly decreases.

Mode 4 (Figure 7d: $t_3 \leq t < t_4$): At $t = t_3$, switch M_2 is in the off state and M_3 is switched on. Since diode D_{M3} is forwardly biased before $t = t_3$, switch M_2 is operated with zero-voltage switching (ZVS) at the turn-on transition. During this time interval, inductor L_S releases energy to the battery. Its current, I_B, linearly decreases.

Mode 5 (Figure 7e: $t_4 \leq t < t_5$): When $t = t_4$, switch M_2 is in the off state and M_3 is switched off. Within this mode, switch current I_{DS3} is a negative value. Diode D_{M3} is forwardly biased to release energy stored in inductor L_s to the battery. Inductor current I_B linearly decreases. When the operational mode is at the end of mode 5, one new switching cycle will start.

B. The utility line source condition: active clamp flyback converter

When the proposed hybrid converter is operated in the utility line source condition, an active clamp flyback converter is used to charge battery. Since the operational state of active clamp flyback converter is always kept in CCM from light load to heavy load, the operational principle of the one is briefly described for CCM operation. According to the operational principle of active clamp flyback converter, its operational mode can be divided into 10 modes. The equivalent circuit of each operational mode is shown in Figure 9 by the blue line, while the conceptual waveforms of each operational mode is illustrated in Figure 10. In the following, each operational mode is briefly explained.

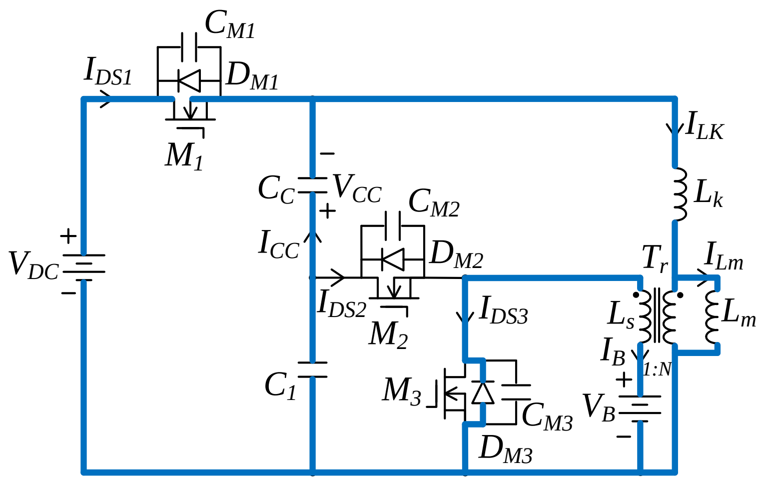

(**a**)

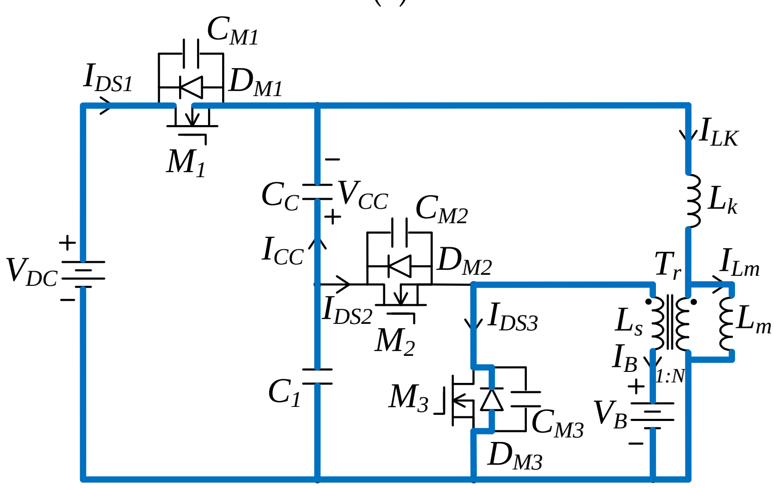

(**b**)

Figure 9. *Cont.*

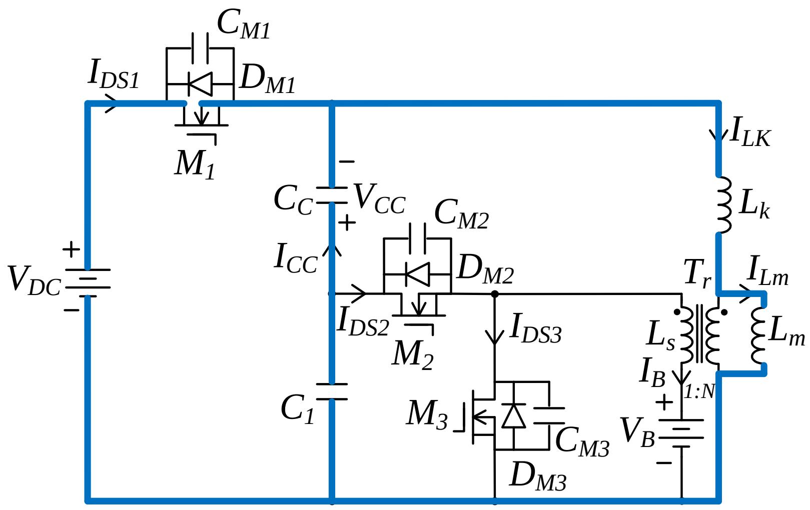

(**c**)

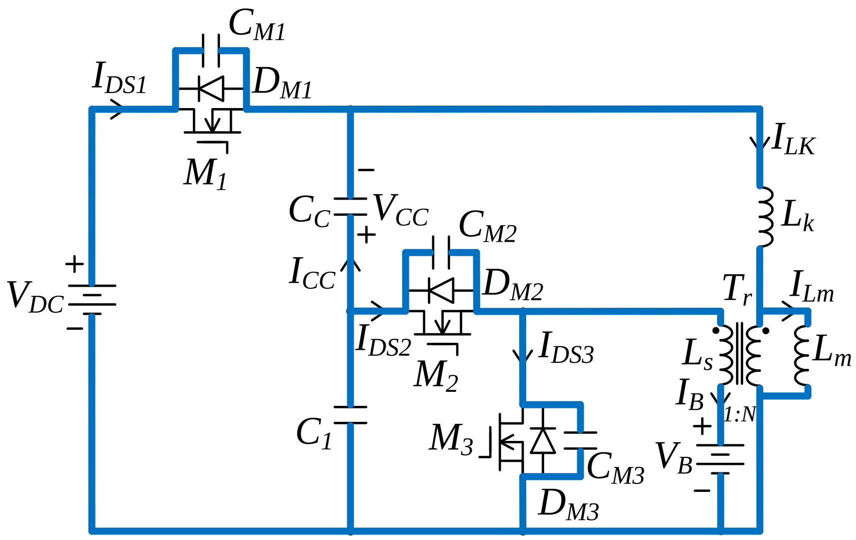

(**d**)

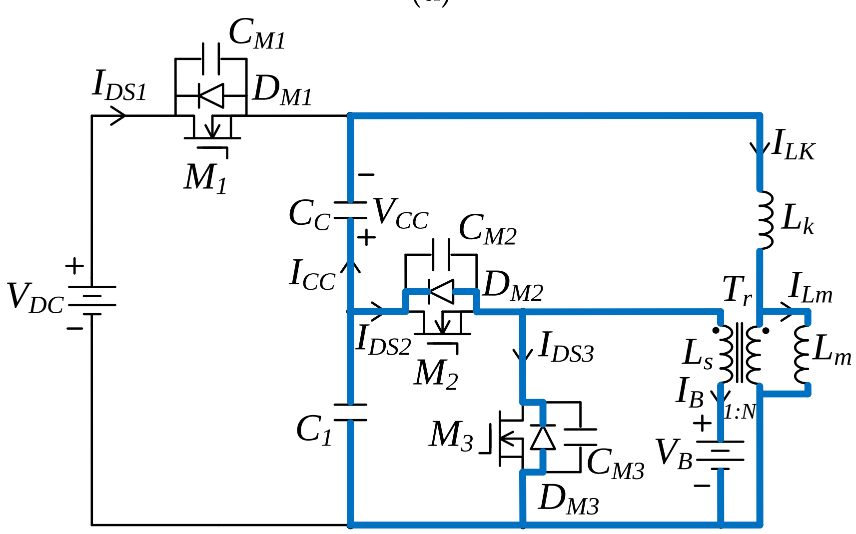

(**e**)

Figure 9. *Cont.*

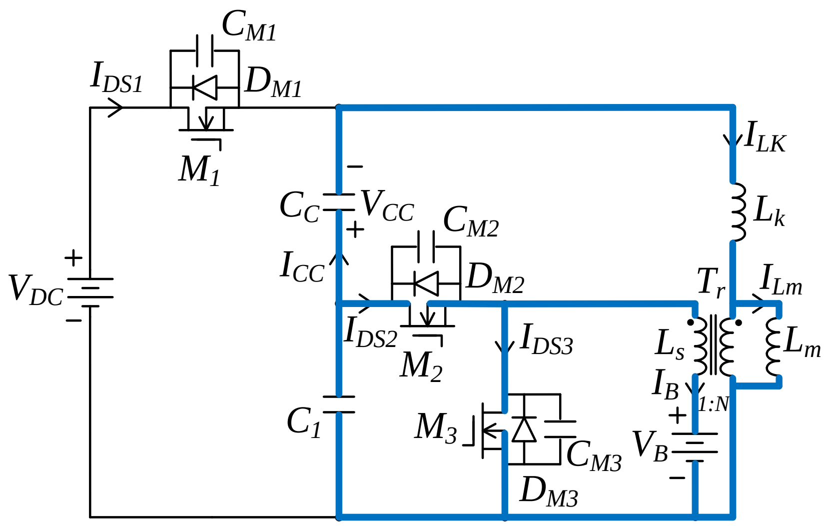

(**f**)

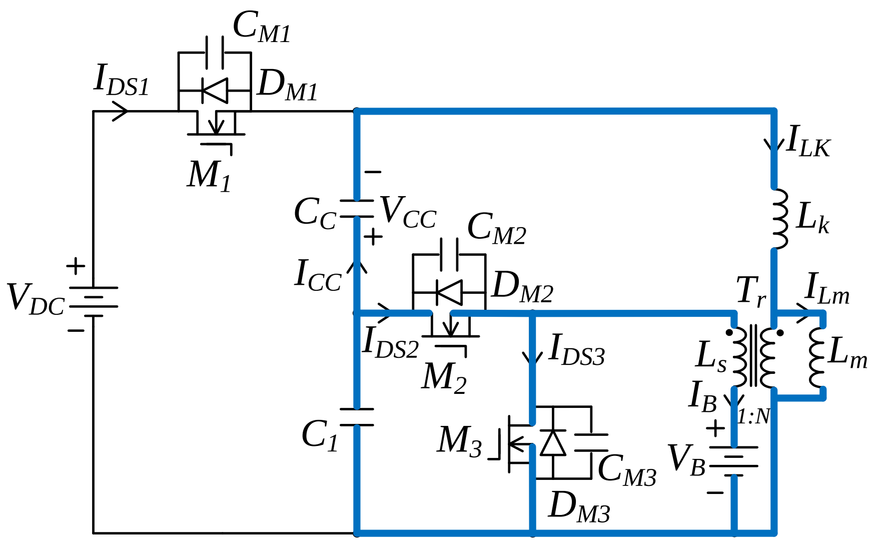

(**g**)

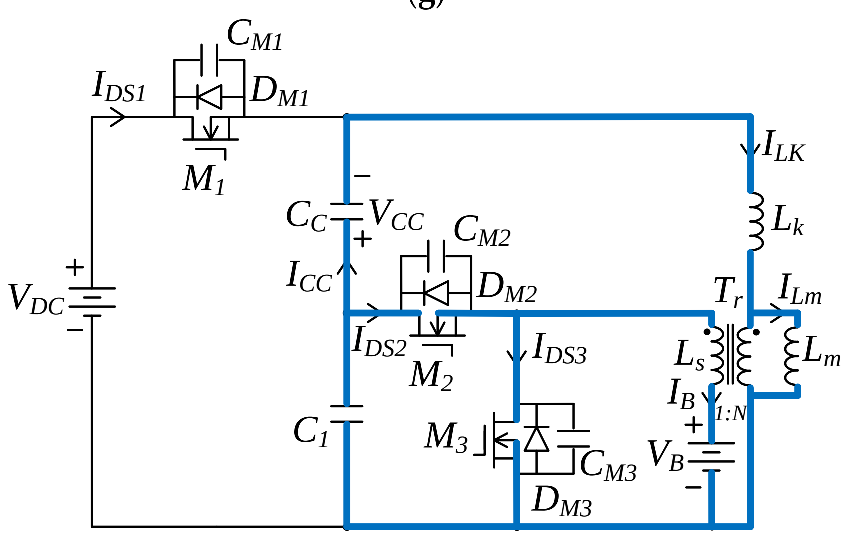

(**h**)

Figure 9. *Cont.*

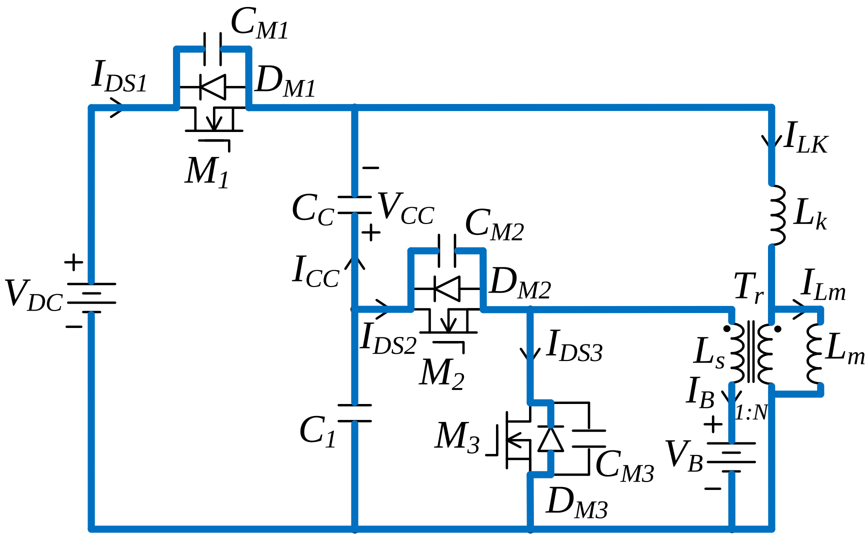

(i)

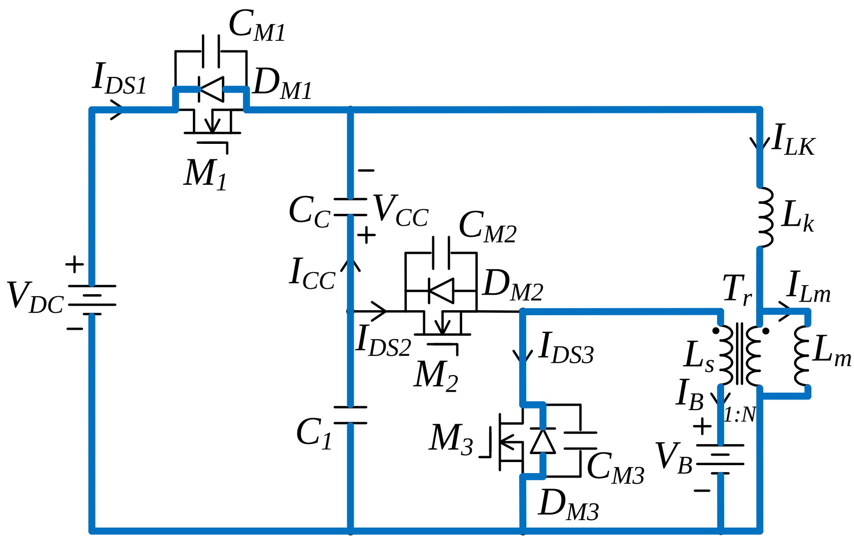

(j)

Figure 9. Equivalent circuit of each operational mode of the proposed hybrid converter operated in the utility line source condition over a complete switching cycle. (**a**) Mode1 ($t_0 \leq t \leq t_1$), (**b**) Mode2 ($t_1 \leq t \leq t_2$), (**c**) Mode3 ($t_2 \leq t \leq t_3$), (**d**) Mode4 ($t_3 \leq t \leq t_4$), (**e**) Mode5 ($t_4 \leq t \leq t_5$), (**f**) Mode6 ($t_5 \leq t \leq t_6$), (**g**) Mode7 ($t_6 \leq t \leq t_7$), (**h**) Mode8 ($t_7 \leq t \leq t_8$), (**i**) Mode9 ($t_8 \leq t \leq t_9$) and (**j**) Mode10 ($t_9 \leq t \leq t_{10}$).

Mode 1 (Figure 9a: $t_0 \leq t < t_1$): Before t_0, switches M_1~M_3 are in the off state, and diodes D_{M1} and D_{M1} are in the forwardly bias state. When $t = t_0$, switch M_1 is switched on, and switches M_2 and M_3 are kept in the off state. At the moment, since diode D_{M1} is forwardly biased before t_0, switch M_1 is operated with ZVS at turn-on transition. During this time interval, current I_{LK} varies from a negative value to 0 A. Since current I_{DS3} is a negative value, diode D_{M3} is in the forwardly bias state. Current I_B linearly decreases and inductor L_m releases energy through transformer T_r and diode D_{M3} to the battery.

Mode 2 (Figure 9b: $t_1 \leq t < t_2$): At t_1, switch M_1 is kept in the on state, and switches M_2 and M_3 are sustained in the off state. Within this mode, inductor current I_{LK} varies from 0 A to the initial value, which is the maximum inductor current of inductor L_m operated in CCM. Moreover, since current I_{DS3} is kept at the negative value, diode D_{M3} is sustained in the forwardly bias state. The magnetizing inductor L_m releases energy to battery.

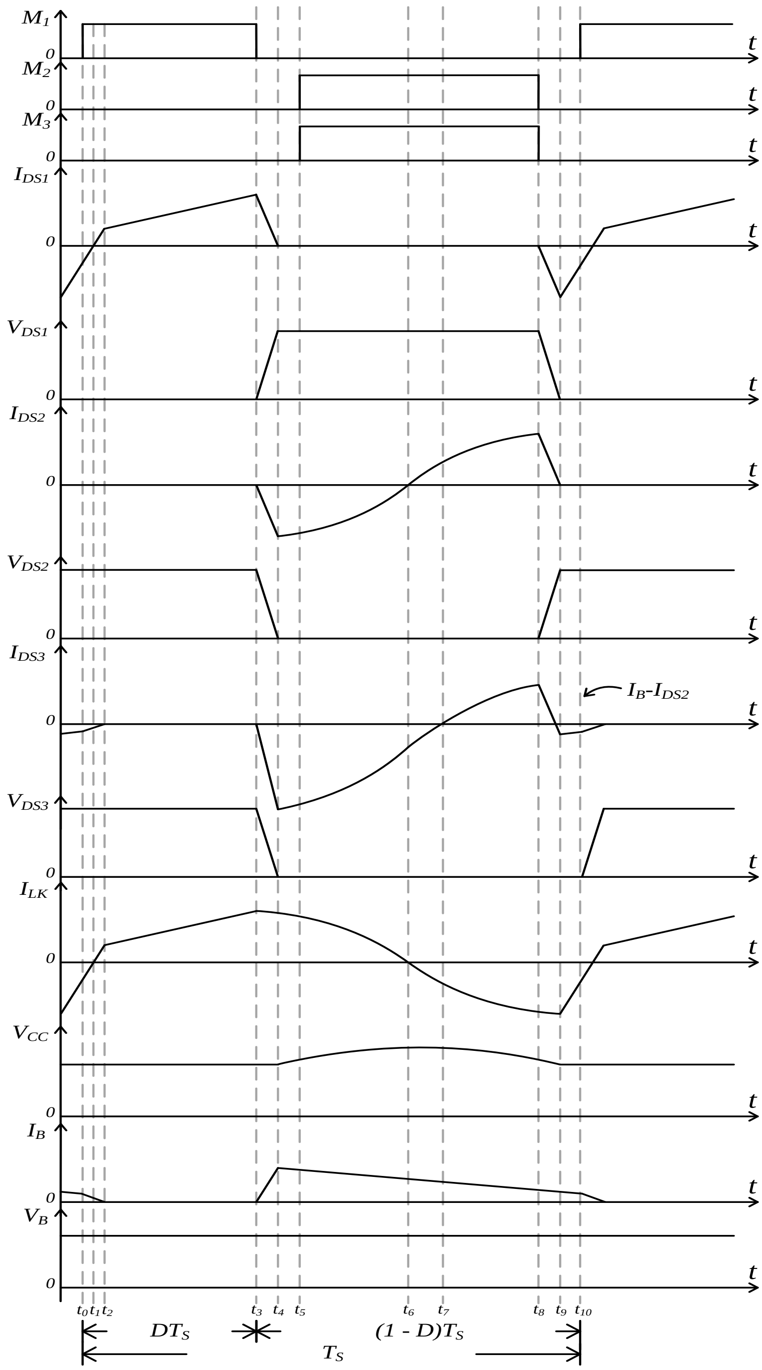

Figure 10. Conceptual waveforms of each operational mode of the proposed hybrid converter operated in the utility line source condition over a complete switching cycle.

Mode 3 (Figure 9c: $t_2 \leq t < t_3$): When $t = t_2$, switch M_1 is sustained in the on state, and switches M_2 and M_3 are in the off state. At the moment, inductor current I_{LK} is equal to current I_{Lm}. Diode D_{M3} is reversely biased. During this time interval, inductor L_m is in the storage energy state. Inductor current I_{Lm} linearly increases.

Mode 4 (Figure 9d: $t_3 \leq t < t_4$): When $t = t_3$, switch M_1 is switched off, and switches M_2 and M_3 are kept in the off state. During this time interval, since inductor current I_{LK} has to be kept in the continuous state, capacitor C_{M1} is charged, and capacitors C_{M2} and C_{M3} are simultaneously discharged. Therefore, voltage V_{DS1} varies from 0 V to [V_{DC} + NV_B].

Voltage V_{DS3} changes from [(V_{DC}/N) + V_B] to 0 V, while voltage V_{DS2} varies from [(N-1)V_B +(N-1)V_{DC}/N] to 0 V.

Mode 5 (Figure 9e: $t_4 \leq t < t_5$): At t_4, switch M_1~M_3 are kept in the off state. In this moment, voltages V_{DS2} and V_{DS3} are equal to 0 V. Diode D_{M2} and D_{M3} are forwardly biased, simultaneously. During this time interval, inductor L_K and capacitor C_C form a resonant network, and they start to generate resonance. Inductor current I_{Lm} releases energy through transformer T_r and diode D_{M3} to battery. I_{Lm} linearly increases.

Mode 6 (Figure 9f: $t_5 \leq t < t_6$): When $t = t_5$, switch M_1 is sustained in the off state, while switches M_2 and M_3 are simultaneously switched on. At the moment, switches M_2 and M_3 are simultaneously operated with ZVS at the turn-on transition. Within this mode, inductor L_K and capacitor C_C are sustained in the resonant state. Current I_{LK} with the resonant manner varies from a maximum negative value to 0 A. Inductor L_m is kept in the released energy state. Therefore, inductor current I_{Lm} linearly increases.

Mode 7 (Figure 9g: $t_6 \leq t < t_7$): When $t = t_6$, switch M_1 is in the off state and switches M_2 and M_3 are kept in the on state. In this moment, current I_{LK} is equal to 0 A. During this time interval, inductor L_K and capacitor C_C are sustained in the resonant state. Inductor L_m releases energy through transformer T_r and switch M_3 to the battery. Therefore, inductor current I_{Lm} linearly increases. Since switch current I_{DS3} is equal to (I_B–I_{DS2}), it varies from a negative value to 0 A.

Mode 8 (Figure 9h: $t_7 \leq t < t_8$): At t_7, switch M_1 is kept in the off state, while switches M_2 and M_3 are simultaneously sustained in the on state. Within this mode, Inductor L_K and capacitor C_C are kept in the resonant state. Inductor current I_{LK} with the resonant manner varies from 0 A to the maximum value. Inductor L_m is in the released energy state. Its value linearly increases.

Mode 9 (Figure 9i: $t_8 \leq t < t_9$): When $t = t_8$, switch M_1 is in the off state, while switches M_2 and M_3 are simultaneously switched on. In this mode, current I_{DS3} is equal to ($-I_B$). Diode D_{M3} is forwardly biased. Since inductor current I_{LK} must be kept in the continuous state, capacitor C_{M1} is discharged, and capacitor C_{M2} is charged. Voltage V_{DS1} varies from [V_{DC} + NV_B] to 0 V, while voltage V_{DS2} changes from 0 V to [($N-1$)V_B +($N-1$)V_{DC}/N]. Inductor L_m is kept in the released energy state.

Mode 10 (Figure 9j: $t_9 \leq t < t_{10}$): At $t = t_9$, switch $M_1 \sim M_3$ are in the off state. At the moment, voltage V_{DS1} is equal to 0 V. Thus, diode D_{M1} is forwardly biased. During this time interval, inductor current I_{LK} varies from the maximum negative value to 0 A. Inductor current L_m is still in the released energy state. When operational mode is at the end of mode 10, one new switching cycle will start.

4. Design of the Proposed Hybrid Converter

Design of the proposed hybrid converter can be divided into two conditions. One is the utility line source condition, and the other is the solar power source condition. In the following, the design of each operational condition is briefly derived.

4.1. The Utility Line Source Condition: Active Clamp Flyback Converter

When the proposed hybrid converter is operated in the utility line source condition, the active clamp flyback converter is adopted to charge lithium battery. Its key parameter design is analyzed in the following.

4.1.1. Duty Ratio D_{11}

Since the active clamp flyback converter does not affect design of duty ratio D_{11} and transformer T_r, the designs of D_{11} and transformer T_r are the same as the conventional flyback converter. According to volt-second balance of magnetizing inductance L_m, the relationship between voltage V_{DC} and output voltage V_B can be expressed as follows:

$$V_{DC}D_{11}T_s + (-NV_B)(1 - D_{11})T_s = 0 \quad (1)$$

where N is turns ratio of transformer T_r, V_{DC} represents the equivalent dc voltage of utility line and T_s expresses the period of switching cycle. From (1), the conversion ratio M_{11} of the active clamp flyback converter can be indicated by the following.

$$M_{11} = \frac{V_B}{V_{DC}} = \frac{D_{11}}{N(1 - D_{11})} \tag{2}$$

When input voltage V_{DC} and battery voltage V_B are specified, duty ratio D_{11} can be rewritten as follows.

$$D_{11} = \frac{NV_B}{NV_B + V_{DC}} \tag{3}$$

In (3), when N is kept at a constant value, the maximum duty ratio $D_{11(max)}$ is determined under the maximum battery voltage $V_{B(max)}$ and minimum input voltage $V_{DC(min)}$. That is, the maximum duty ratio $D_{11(max)}$ is determined by the following.

$$D_{11(max)} = \frac{NV_{B(max)}}{NV_B(max) + V_{DC(\min)}} \tag{4}$$

In general, if the maximum duty ratio of a pulse-width modulation integrated circuit (PWM IC) is limited within 0.5, the maximum duty ratio $D_{11(max)}$ has better selection ranges from 0.35 to 0.4.

4.1.2. Transformer T_r

For the design of transformer T_r, turn ratio N and magnetizing inductance L_m are two key parameters. In (4), when the maximum duty ratio $D_{11(max)}$, battery voltage $V_{B(max)}$ and input voltage $V_{DC(min)}$ are determined, turns ratio N can be rewritten by the following.

$$N = \frac{D_{11(max)} V_{DC(\min)}}{(1 - D_{11(max)}) V_{B(max)}}. \tag{5}$$

In order to design magnetizing inductance L_m, magnetizing inductor current variation ΔI_{Lm1} must be determined. In general, when the proposed flyback converter is operated in the boundaries of CCM and discontinuous conduction mode (DCM), average current $I_{B1(av)}$ can be obtained as the desired reference value. Ratio K_1 of the average current $I_{B1(av)}$ to the maximum charging current $I_{B(max)}$ is set. That is, when the proposed converter begins to enter CCM operation, the average current $I_{B1(av)}$ is equal to $K_1 I_{B(max)}$, where K_1 varies from 0 to 1. Figure 11 plots ideal waveforms of inductor current I_{Lm} and charging current I_{B1} of the proposed one operated at the boundary condition. In Figure 11, the average current $I_{B1(av)}$ is expressed by the following.

$$I_{B1(\mathrm{av})} = \frac{N \Delta I_{Lm1} (1 - D_{11})}{2}. \tag{6}$$

In Figure 11, current variation ΔI_{Lm1} is equal to $I_{Lm(P)}$. According to operational principle of the proposed flyback converter, current variation ΔI_{Lm1} can be derived as follows:

$$\Delta I_{Lm1} = I_{Lm(P)} = \frac{V_{DC} D_{11} T_s}{L_{mB1}}, \tag{7}$$

where L_{mB1} is the boundary value of magnetizing inductance L_{m1} when the proposed flyback converter is operated in the boundary of CCM and DCM. Since the proposed one adopts the active clamp circuit to achieve ZVS operational features under CCM condition, it magnetizing inductance L_{m1} is always operated in CCM to increase soft-switching operational ranges. In order to achieve a variety of soft-switching operational ranges, the proposed one begins to enter CCM under light load conditions. From (6) and (7), the magnetizing inductance L_{m1} can be expressed as follows.

$$L_{m1} = \frac{NV_{DC}D_{11}(1 - D_{11})T_s}{2K_1 I_{B(max)}}. \quad (8)$$

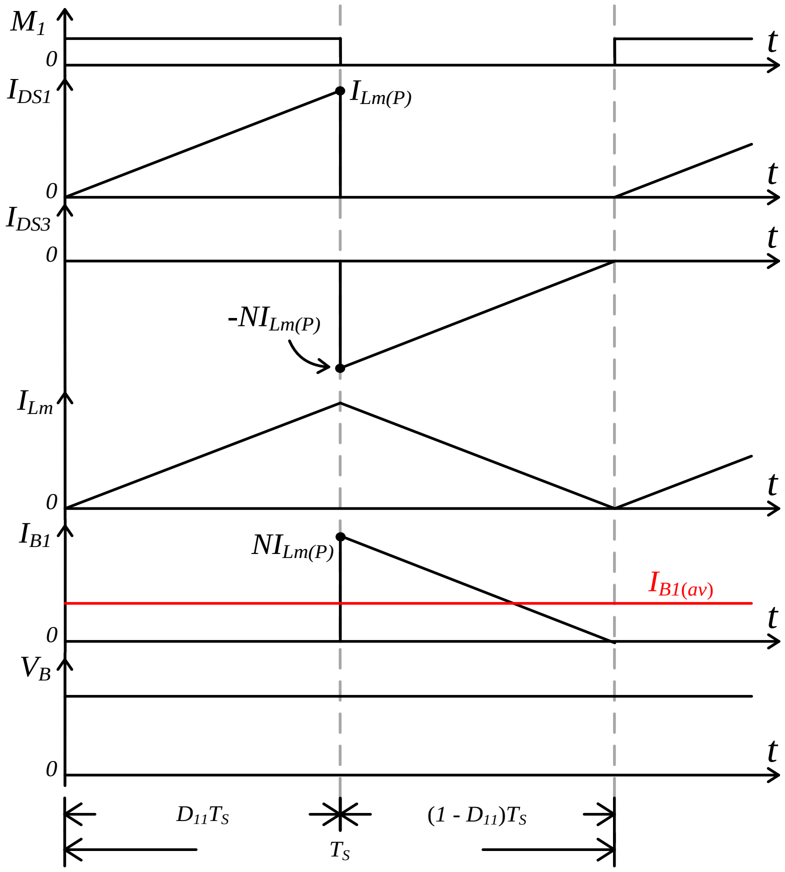

Figure 11. Ideal waveforms of inductor current I_{Lm} and charging current I_{B1} of the proposed flyback converter operated in the boundary of CCM and DCM.

4.1.3. Capacitor C_c

In the active clamp flyback converter, capacitor C_c is adopted to recover energy stored in leakage inductance L_K and achieve ZVS features of switches. Since inductor L_K and capacitor C_c are connected in series to form a resonant network, half of the resonant period is equal to or greater than the turn-off time of switch M_1 to produce a wider range of soft-switching features. Thus, capacitor C_c has to satisfy the following inequality.

$$\pi\sqrt{L_K C_c} \geq (1 - D_{11})T_s. \quad (9)$$

In (9), capacitor C_c can be rewritten as follows.

$$C_c \geq \frac{(1 - D_{11})^2 T_s^2}{\pi^2 L_K} \quad (10)$$

From (5) and (8), magnetizing inductor L_{m1} and turn ratio N of transformer T_r can be obtained, and then the turns of primary and secondary windings of transformer T_r can be determined. According to the turns of primary and secondary windings relative to wind transformer T_r, leakage inductance L_K can be measured by the practical wound transformer T_r. When leakage inductance L_K is obtained, capacitor C_c can be also determined by (10).

4.2. The Solar Power Source Condition: Buck Converter

When a battery uses solar power as its input source, the buck converter is regarded as the battery charger, as shown in Figure 6a. To design the proposed buck converter, the key parameters are derived in the following.

4.2.1. Duty Ratio D_{12}

In Figure 6a, switch M_2 is regarded as the main switch of the proposed buck converter, while switch M_3 is used as the auxiliary switch. According to volt-second balance of inductor L_s, its relationship is expressed by the following:

$$(V_{PV} - V_B)D_{12}T_s + (-V_B)(1 - D_{12})T_s = 0, \tag{11}$$

where V_{PV} is output voltage of solar power, V_B represents battery voltage and T_s expresses the period of switching cycle. Conversion ratio M_{12} of the proposed buck converter can be analyzed as follows.

$$M_{12} = \frac{V_B}{V_{PV}} = D_{12}. \tag{12}$$

From (12), the maximum duty ratio $D_{12(max)}$ happens at the maximum battery voltage $V_{B(max)}$ and minimum voltage $V_{PV(min)}$. Therefore, the maximum duty ratio $D_{12(max)}$ can be determined by the following.

$$D_{12(max)} = \frac{V_{B(max)}}{V_{PV(\min)}}. \tag{13}$$

When the proposed hybrid converter is operated in the solar power condition, the proposed one can regulate output current with CC method to charge lithium battery and extract maximum output power of solar power. Its duty ratio D_{12} is limited within $D_{12(max)}$, as illustrated in (13).

4.2.2. Inductor L_s

Inductor L_s is the inductance of secondary winding of transformer T_r. Its value is equal to (L_{m1}/N^2). Figure 12 shows ideal waveforms of current I_{DS2}, I_{DS3} and I_{B2} of the proposed buck converter operated in the boundaries of CCM and DCM. From Figure 12, the average charging current $I_{B2(av)}$ can be derived by the following:

$$I_{B2(av)} = \frac{\Delta I_{LS}}{2} = \frac{I_{LS(P)}}{2}, \tag{14}$$

where ΔI_{LS} is the current variation of inductor L_s, and $I_{LS(P)}$ expresses the peak current of inductor L_s. Since voltage V_{LS} across inductor L_s is equal to (V_{PV} – V_B) during switch M_2 in the on state, current $I_{LS(P)}$ can be the inductor as follows:

$$I_{LS(P)} = \frac{(V_{PV} - V_B)}{L_{SB}} D_{12}T_S, \tag{15}$$

where L_{SB} is the boundary inductance of L_S when the proposed converter is operated in the boundary of CCM and DCM. In (13), when the maximum voltage $V_{B(max)}$ and minimum voltage $V_{PV(min)}$ are specified, the maximum duty ratio $D_{12(max)}$ can be obtained. Therefore, inductor current $I_{LS(P)}$ can be rewritten as follows.

$$I_{LS(P)} = \frac{\left(V_{PV(\min)} - V_{B(max)}\right)}{L_{SB}} D_{12(max)}T_S. \tag{16}$$

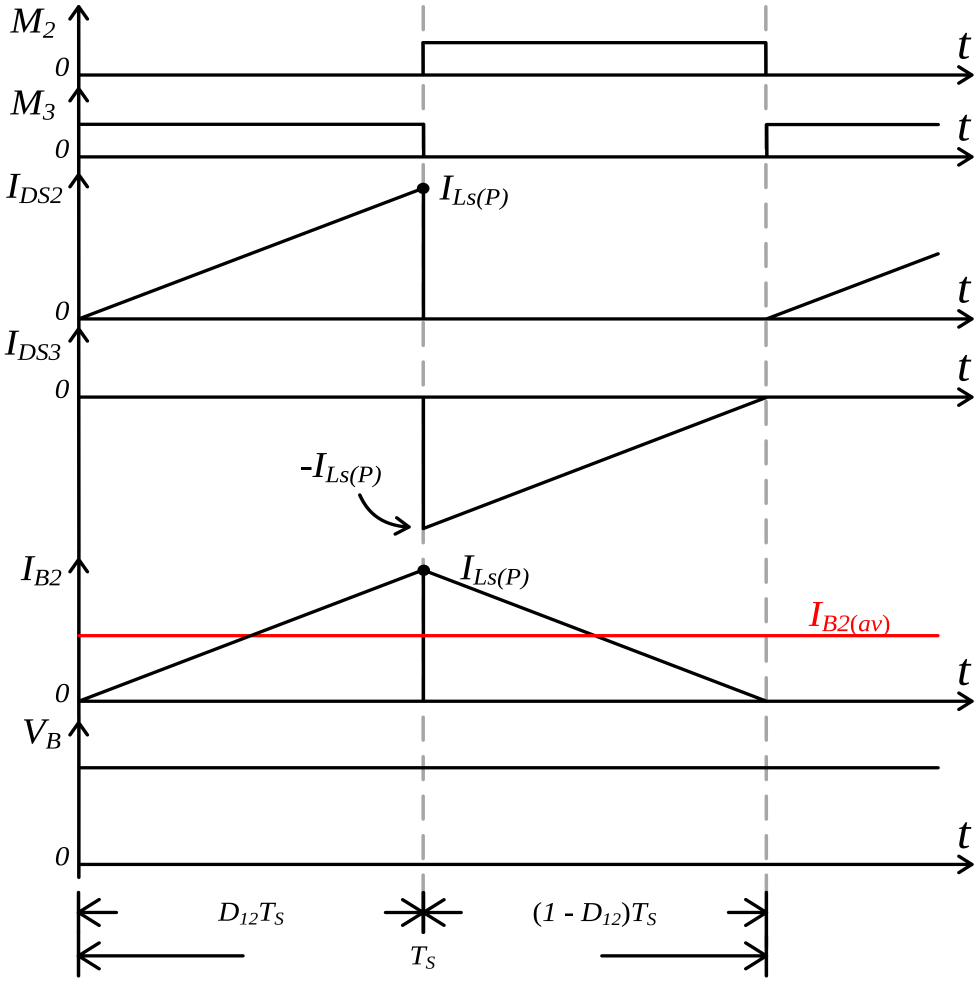

Figure 12. Ideal waveforms of inductor current I_{DS2}, I_{DS3} and I_{B2} of the proposed buck converter operated in the boundary of CCM and DCM.

From (14) and (15), the average current $I_{B2(av)}$ is as follows.

$$I_{B2(av)} = \frac{\left(V_{PV(\min)} - V_{B(max)}\right)}{2L_{SB}} D_{12(max)} T_S. \quad (17)$$

When the proposed buck converter is operated in the boundary, average current $I_{B2(av)}$ is set at $K_2 I_{B(max)}$, where K_2 varies from 0 to 1, and $I_{B(max)}$ expresses the maximum charging current. In general, K_2 has a better selection range under 0.2~0.3. Therefore, inductor L_s can be expressed by the following.

$$Ls = \frac{\left(V_{PV(\min)} - V_{B(max)}\right)}{2K_2 I_{B(max)}} D_{12(max)} T_S. \quad (18)$$

Since inductor L_s is equal to (L_{m2}/N^2), inductor L_{m2} can be indicated by the following.

$$L_{m2} = \frac{N^2\left(V_{PV(\min)} - V_{B(max)}\right)}{2K_2 I_{B(max)}} D_{12(max)} T_S. \quad (19)$$

In order to design the proposed hybrid converter, inductor L_m of transformer T_r can be determined by inductors L_{m1} and L_{m2}. It can be selected with the larger value between L_{m1} and L_{m2}.

5. Control Circuit of the Proposed Hybrid Converter

The proposed hybrid converter adopts the utility line and solar power as its input source, respectively. In order to achieve a power supply system with multiple sources, the proposed one needs a controller to implement battery charging control and MPPT functions. Figure 13 illustrates the block diagram of the controller for the proposed hybrid converter. In Figure 13, the proposed one is divided into two parts: power circuit and controller. The controller is used to control power circuit for supplying power to battery. Therefore, the controller includes MPPT, power source selection, CC command selection, CC/CV command, PWM generator and battery protection units. Table 2 lists definitions of key parameters in Figure 13, while Table 3 illustrates the operational condition of the proposed hybrid converter. In the following, each control unit is briefly described.

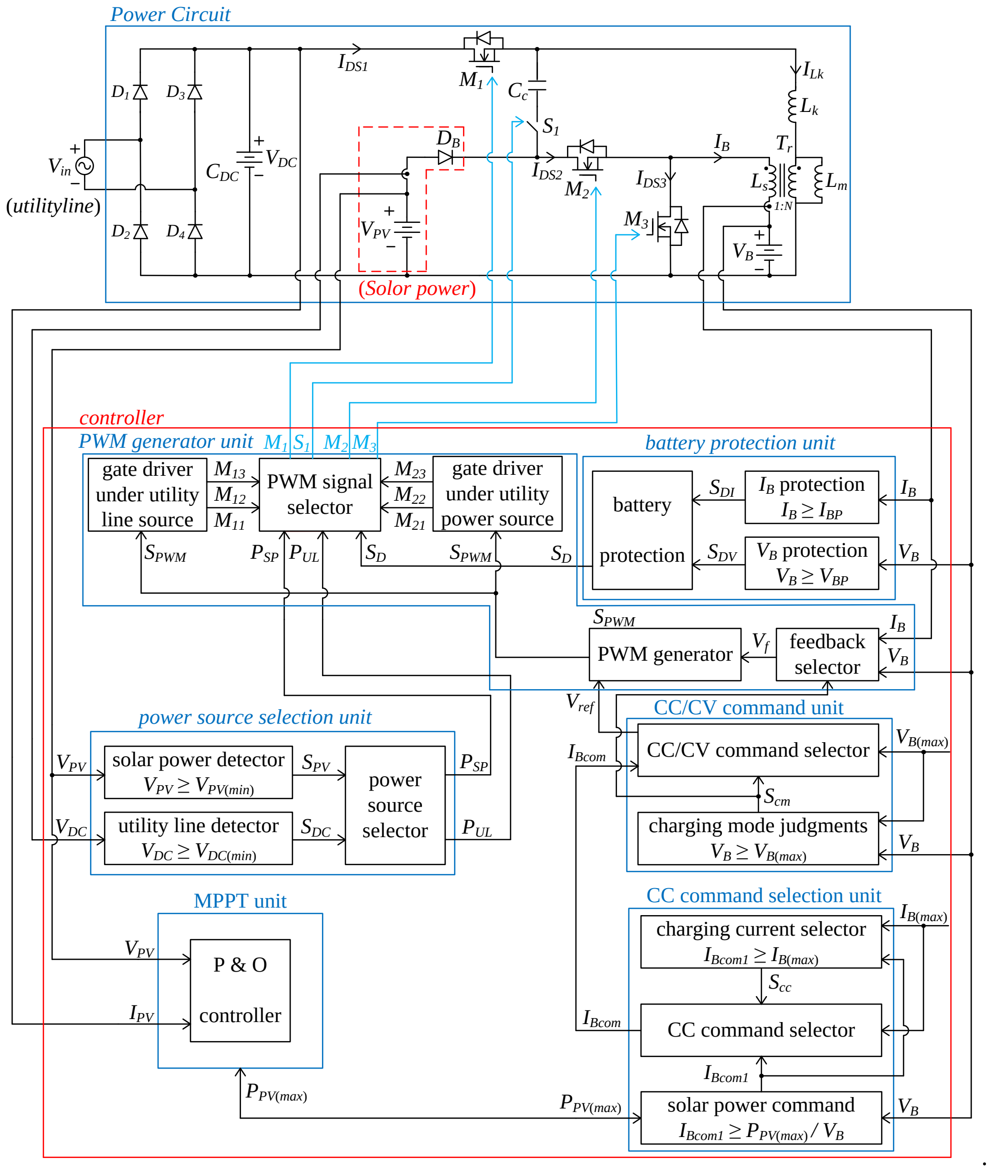

Figure 13. Block diagram of controller for the proposed hybrid converter.

Table 2. Definitions of key parameters in Figure 13 for the controller of the proposed hybrid converter.

Symbol	Definition	Symbol	Definition
V_{PV}	output voltage of solar power	S_{DI}	protection signal of $I_B \geq I_{BP}$
$V_{PV(min)}$	minimum output voltage of solar power	S_{DV}	protection signal of $V_B \geq V_{BP}$
V_{DC}	equivalent dc voltage of utility line	S_D	protection signal of battery
$V_{DC(min)}$	minimum equivalent dc voltage of utility line	S_{PV}	detector signal of $V_{PV} \geq V_{PV(min)}$
V_B	battery voltage	S_{DC}	detector signal of $V_{DC} \geq V_{DC(min)}$
$V_{B(max)}$	maximum battery voltage	P_{SP}	selector signal of solar power
V_{BP}	voltage protection of battery	P_{UL}	selector signal of utility line
I_B	Battery current	M_{11}	gate signal of switch M_1 under utility line source
$I_{B(max)}$	maximum charging current of Battery	M_{12}	gate signal of switch M_2 under utility line source
I_{BP}	current protection of battery	M_{13}	gate signal of switch M_3 under utility line source
$P_{PV(max)}$	maximum output power of solar power at present	M_{21}	gate signal of switch M_1 under solar power source
I_{Bcom1}	current command value under $P_{PV(max)}$	M_{22}	gate signal of switch M_2 under solar power source
I_{Bcom}	current command value with CC charging method	M_{23}	gate signal of switch M_3 under solar power source
S_{cc}	selecting signal of CC command	M_1	gate signal of switch M_1
S_{cm}	selecting signal of CC/CV command	M_2	gate signal of switch M_2
V_{ref}	command signal of PWM generator	M_3	gate signal of switch M_3
V_f	feedback signal of PWM generator	S_1	gate signal of switch S_1
S_{PWM}	PWM signal of main switch generator		

Table 3. Operational condition of the proposed hybrid converter for the controller shown.

Controlling Unit		Selection/Judgement Condition		Operational Condition
		Variable	State	
Power source selection unit	solar power detector	S_{PV}	High	$V_{PV} \geq V_{PV(min)}$
			Low	$V_{PV} < V_{PV(min)}$
	utility line detector	S_{DC}	High High	$V_{DC} \geq V_{DC(min)}$
			Low Low	$V_{DC} < V_{DC(min)}$
	power source selector	P_{SP}	High	under the solar power condition
			Low	Shutdown solar power
		P_{SP}	High	under the solar utility line condition
			Low Low	Shutdown utility line
CC command selection unit	solar power command	I_{Bcom1}		$I_{Bcom1} = \frac{P_{PV(max)}}{V_B}$
	Charging current selector	S_{cc}	High	$I_{Bcom1} \geq I_{B(max)}$
			Low	$I_{Bcom1} < I_{B(max)}$
	CC command selector	I_{Bcom}	S_{cc} = High	$I_{Bcom} = I_{B(max)}$
			S_{cc} = Low	$I_{Bcom} = I_{Bcom1}$

Table 3. *Cont.*

Controlling Unit		Selection/Judgement Condition		Operational Condition
		Variable	State	
CC/CV command unit	Charging mode judgement	S_{cm}	High	$V_B \geq V_{B(max)}$
			Low	$V_B < V_{B(max)}$
	CC/CV command selector	V_{ref}	S_{cm} = High	$V_{ref} = V_{B(max)}$ under CV operation
			S_{cm} = Low	$V_{ref} = I_{B\text{com}}$ under CC operation
PWM generator unit	Feedback selector	V_f	S_{cm} = High	$V_f = V_B$ under CV operation
			S_{cm} = Low	$V_f = I_B$ under CC operation
	PWM generator	S_{PWM}		Error value by V_{ref} and V_f
	Gate driver	M_{11}		$M_{11} = S_{PWM}$
	under utility	M_{12}		$M_{12} = \overline{S_{PWM}}$
	line source	M_{13}		$M_{13} = \overline{S_{PWM}}$
	Gate driver	M_{21}		turn-off
	under solar	M_{22}		$M_{22} = S_{PWM}$
	power source	M_{23}		$M_{23} = \overline{S_{PWM}}$
	PWM signal selector	M_1		$M_1 = P_{UL}\, M_{11} + P_{SP}\, M_{21}$
		M_2		$M_2 = P_{UL}\, M_{12} + P_{SP}\, M_{22}$
		M_3		$M_3 = P_{UL}\, M_{13} + P_{SP}\, M_{23}$
		S_1	P_{SP} = High	S_1 = Low
			P_{UL} = High	S_1 = High
		S_D	High	shutdown the proposed hybrid converter
			Low	normal operation
Battery protection unit	I_B protection	S_{DI}	High	$I_B \geq I_{BP}$
			Low	$I_B < I_{BP}$
	V_B protection	S_{DV}	High	$V_B \geq V_{BP}$
			Low	$V_B < V_{BP}$
	battery protection	S_D		$S_D = S_{DI} + S_{DV}$

5.1. MPPT Unit

The proposed hybrid converter possesses two operational conditions: the utility line source and solar power source conditions. When the proposed one uses solar power as its input source, it regulates charging current I_B with the CC method to charge the battery and implement MPPT. For implementing MPPT of solar power, the perturb and observe algorithm (P&O) was used for tracking the maximum power point (MPP) of solar power [27]. Since its algorithm is described in [27], it will not be described in this paper. As mentioned above, the MPPT unit in the controller adopts voltage V_{PV} and current I_{PV} to obtain the maximum power $P_{PV\,(max)}$ of solar power.

5.2. CC Command Selection Unit

When the proposed hybrid converter is operated for a battery charger, charging current I_B uses the CC-CV method to supply power to the battery. In order to implement the battery charging function with the CC method, the controller must generate CC command value I_{BCOM} to regulate charging current I_B. The CC command selection unit is used to generate CC command value I_{BCOM}. When the maximum power $P_{PV(max)}$ of solar power is obtained, the solar power command can produce a command value I_{BCOM1}, which can be expressed by ($P_{PV(max)}/V_B$). Since the charging current I_B is limited within $I_{B(max)}$, charging the current selector can generate control signal S_{CC}, which is obtained by the relationship between I_{BCOM1} and $I_{B(max)}$. When $I_{BCOM1} \geq I_{B(max)}$, signal S_{CC} varies from low levels to high levels. It is used to control the CC command selector, and signal I_{BCOM} is equal to $I_{B(max)}$. If I_{BCOM1} $< I_{B(max)}$, signal S_{CC} is kept at low levels. It can control CC command selector to obtain $I_{BCOM} = I_{BCOM1}$.

Since the battery charging method adopts the CC–CV hybrid method to obtain better charging efficiency, the CC/CV command unit can produce a selecting signal S_{Cm} to control the battery charger operated in the CC charging mode or the CV charging mode. When voltage V_B is equal to or greater than voltage $V_{B(max)}$, signal S_{Cm} varies from low levels to high levels. The proposed battery charger is operated in the CV charging mode. The command value V_{ref} is equal to $V_{B(max)}$. Moreover, the feedback selector can induce feedback signal V_f, which is equal to V_B. The error value can be obtained by difference between the command value V_{ref} and feedback value V_f when signals V_{ref} and V_f are sent to PWM generator for generating error value. The error value compared with a triangle wave in the PWM generator can produce signal S_{PWM} to drive switches in the proposed hybrid converter for battery charging. In addition, when $V_B < V_{B(max)}$, the proposed one is operated in the CC charging mode. Signal $V_{ref} = I_{BCOM}$ and $V_f = I_B$. PWM generator can receive signals V_{ref} and V_f to generate S_{PWM} for battery charging.

5.3. PWM Generator Unit

The PWM generator unit includes a feedback selector, PWM generator, gate driver under utility line source, gate driver under solar power source and PWM signal selector. The feedback selector and PWM generator receives command value V_{ref} and feedback value V_f to generate PWM signal S_{PWM} for implementing CC or CV charge. The PWM signal S_{PWM} can be sent to gate driver under utility line source and gate driver under solar power source for generating different PWM signals under different power source to implement battery charger.

In the gate driver under utility line source, the PWM signal S_{PWM} is sent to this control circuit to generate three PWM signals. The PWM signal M_{11} is used to drive switch M_1, which is regarded as the main switch. PWM signals M_{11} and M_{12} are operated in complementary, while PWM signals M_{12} and M_{13} are operated synchronously. Switches M_2 and M_3 are regarded as auxiliary switches and are driven by PWM signals M_{12} and M_{13}, respectively. In addition, the gate driver under the solar power source can produce three PWM signals, M_{21}, M_{22} and M_{23}, by PWM signal S_{PWM}. PWM signal M_{22} is the main PWM signal for driving switch M_2. The PWM signals M_{22} and M_{23} are operated complementarily. Therefore, PWM signal M_{23} is used to drive auxiliary switch M_3. In this operational condition, signal M_{21} is switched off. Two pairs of PWM signals (M_{11}, M_{12}, M_{13}) and (M_{21}, M_{22}, M_{23}) are sent to a PWM signal selector to produce PWM signals selector to produce PWM signals M_1, M_2 and M_3. When operational signal P_{SP} is in the high level, PWM signals, $M_1 = M_{11}$, $M_2 = M_{12}$, $M_3 = M_{13}$, are adopted to drive switches M_1, M_2 and M_3, respectively. During this operational condition, the proposed hybrid converter is operated in the solar power source condition. Switch S_1 is switched off. If operational signal P_{UL} is in the high level, PWM signals $M_1 = M_{21}$, $M_2 = M_{22}$ and $M_3 = M_{23}$ are used to drive switches M_1, M_2 and M_3 separately. Within this operational condition, utility line source is regarded as the input source of the proposed hybrid converter. Switch S_1 is switched on. Moreover, signal S_D is the shutdown signal of the proposed hybrid converter.

When signal S_D is in the high level, the proposed one enters the shutdown condition. During this time interval, battery operational condition is under $I_B \geq I_{BP}$ or $V_B \geq V_{BP}$.

5.4. Power Source Selection Unit

A power source selection unit is used to select power source as input source of the proposed hybrid converter. When solar power can supply enough power to battery, the proposed one can use solar power to supply power for the battery. During this operational condition, the solar power detector is in the $V_{PV} \geq V_{PV(min)}$ condition. Signal S_{PV} is in the high level. Therefore, signal P_{SP} is under the high level, and signal P_{UL} is in the low level. If $V_{PV} \geq V_{PV(min)}$ and $V_{DC} \geq V_{DC\,(min)}$, signals S_{PV} and S_{DC} are simultaneously in the high level. When $V_{PV} \geq V_{PV(min)}$ and $V_{DC} \geq V_{DC\,(min)}$, signals S_{PV} and S_{DC} are simultaneously in the high level. Within this operational condition, the powers of solar power and utility line are large enough to supply power to battery. Since the power source in the proposed hybrid converter is a priority selection to solar power, the proposed one is operated in the solar power condition. Signal P_{SP} is in the high level state. In addition, when $V_{PV} < V_{PV(min)}$ and $V_{DC} \geq V_{DC\,(min)}$, solar power is not enough to supply power to the battery, and the utility line is large enough to supply power to battery. Therefore, a utility line can supply power to the battery. Signal P_{UL} is in the high level state. When $V_{PV} < V_{PV(min)}$ and $V_{DC} < V_{DC\,(min)}$, solar power and utility lines are not enough to supply power to battery, simultaneously. Signals P_{SP} and P_{UL} are under the low level state. The proposed hybrid converter is operated in the shutdown condition. The operational condition of the proposed one is listed in Table 3.

5.5. Battery Protection Unit

The battery does not operate in overcurrent and overvoltage conditions. When $I_B \geq I_{BP}$, the charging current I_B is greater than the maximum charging current $I_{B(max)}$. Signal S_{DI} is in the high level state, and the proposed hybrid converter must be shut down. If $V_B \geq V_{BP}$, battery voltage V_B is greater than maximum charging voltage $V_{B(max)}$. Signal S_{DV} is in the high level state, and the proposed one can be shut down. Therefore, shutdown signal S_D is equal to S_{DI} + S_{DV}. When signal S_D is in the high level state, the proposed hybrid converter is operated in the shutdown condition.

6. Experimental Results

The proposed hybrid converter can be operated in the utility line source and solar power source conditions. In order to verify battery charging features, a prototype was implemented with the following specifications:

A. The utility line source condition: active clamp flyback converter

- Input voltage V_{DC}: DC127~183 V (AC90 V~130 V);
- Switching frequency f_{s1}: 50 kHz;
- Output voltage V_B: DC5 V~8.4 V (battery pack: 2 series*8 parallel);
- Maximum charging current $I_{B(max)}$: 12 A.

B. The solar power source condition: buck converter

- Input voltage V_{PV}: DC30~45 V (solar panel: $P_{PV(max)}$ = 100 W);
- Switching frequency f_{s2}: 50 kHz;
- Output voltage V_B: DC5 V~8.4 V (battery pack: 2 series*8 parallel);
- Maximum charging current $I_{B(max)}$: 12 A.

According to the previous specifications of the proposed hybrid converter operated in different power source conditions, the specifications of solar power is illustrated in Table 4, from which it can be observed that maximum output power $P_{PV(max)}$ = 100 W, maximum power voltage V_{PV} = 36 V and maximum power current I_{PV} = 2.78 A. In addition, the battery pack includes 16 sets of battery cells. Specifications of each battery cell are illustrated in Table 5. Two battery cells connected in series are regarded as a string. Eight sets of strings compose battery pack. In Table 5, the voltage of the battery pack varies from

5 V to 8.4 V, and the maximum charging current $I_{B(max)}$ is equal to 12 A. Therefore, the battery pack is expressed by two series*8 parallel.

Table 4. Specifications of solar panel.

Parameters	Single Module Value	Series Module Value
Maximum Power $P_{PV(max)}$	50 W	100 W
Open circuit voltage V_{DC}	22.5 V	45 V
Maximum Power voltage $V_{PV(max)}$	17.96 V	36 V
Maximum Power current $I_{PV(max)}$	2.78 A	2.78 A
Short circuit current I_{SC}	3.1 A	3.1 A

Table 5. Specifications of lithium battery.

Parameters	Single Battery Cell		Battery Pack: 2 Series *8 Parallel	
	Rated Value	Practical Value	Rated Value	Practical Value
Rated capacity	3.2 Ah	3.2 Ah	25.6 Ah	25.6 Ah
Nominal voltage $V_{B(NV)}$	3.6 V	3.6 V	7.2 V	7.2 V
Maximum voltage $V_{B(max)}$	4.2 V	4.2 V	8.4 V	8.4 V
Protection voltage V_{BP}		4.3 V		8.6 V
Maximum charging current $I_{B(max)}$	1.625 A	1.5 A	6.5 A	6 A
Protection current I_{BP}		1.6 A		6.4 A
Maximum discharging current $I_{BD(max)}$	6.4 A		25.6 A	
Minimum discharging voltage $V_{B(min)}$	2.5 V	2.5 V	5 V	5 V

According to the design of the proposed hybrid converter, the key components are listed in Table 6. In order to verify the performances of the proposed hybrid converter, the experimental results are separately measured under solar power and utility line conditions. When solar voltage P_{PV} = 36 V, the measured switch voltage V_{DS} and current I_{DS} waveforms of switches M_2 and M_3 are shown in Figures 14 and 15. Figure 14 shows those waveforms under 25% of the full-load condition, while Figure 15 depicts those waveforms under 100% of the full-load condition. From Figures 14 and 15, it can be observed that the proposed hybrid converter can adopt solar power to charge battery from light load to heavy load. Figure 16 illustrates measured battery voltage V_B and current I_B waveforms under different charging currents. When charging current I_B = 3 A, those waveforms are shown in Figure 16a. In addition, when I_B = 6 A, those waveforms are expressed in Figure 16b. From measured voltage V_B and current I_B waveforms, the proposed hybrid converter operated in the solar power condition can achieve different charging currents under a constant value.

Table 6. Key components of the proposed hybrid converter.

Symbol	Material Type	Power Rating/Value
Switch M_1	STF13NM60N	650 V/11 A
Switch M_2	STO36N60M6	600 V/30 A
Switch M_3	AOW2918	100/90 A
Switch S_1	STF13NM60N	650 V/11 A
Capacitor C_c	Mpp Capacitor	0.4 F/400 V
Transformer T_r	EE-33 CORE	L_m = 3.6 mH, L_K = 40μH, N = 9

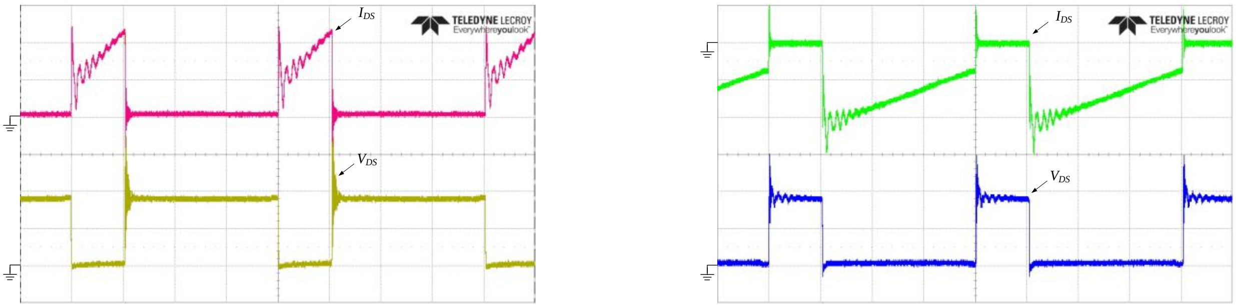

(**a**) (I_{DS}: 2 A/div, V_{DS}: 20 V/div, time: 5 µs/div) (**b**) (I_{DS}: 2 A/div, V_{DS}: 20 V/div, time: 5 µs/div)

Figure 14. Measured waveforms of switch voltage V_{DS} and current I_{DS} under 25% of the full-load condition when V_{PV} = 36 V: (**a**) switch M_2 and (**b**) switch M_3.

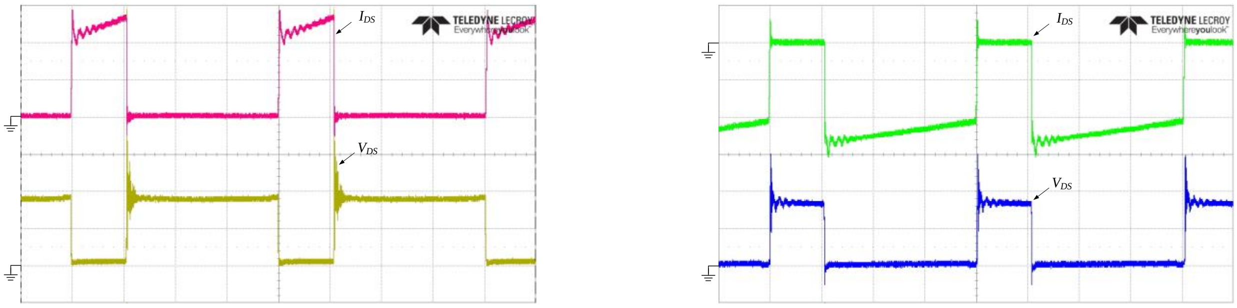

(**a**) (I_{DS}: 5 A/div, V_{DS}: 20 V/div, time: 5 µs/div) (**b**) (I_{DS}: 5 A/div, V_{DS}: 20 V/div, time: 5 µs/div)

Figure 15. Measured waveforms of switch voltage V_{DS} and current I_{DS} under 100% of the full-load condition when V_{PV} = 36 V: (**a**) switch M_2 and (**b**) switch M_3.

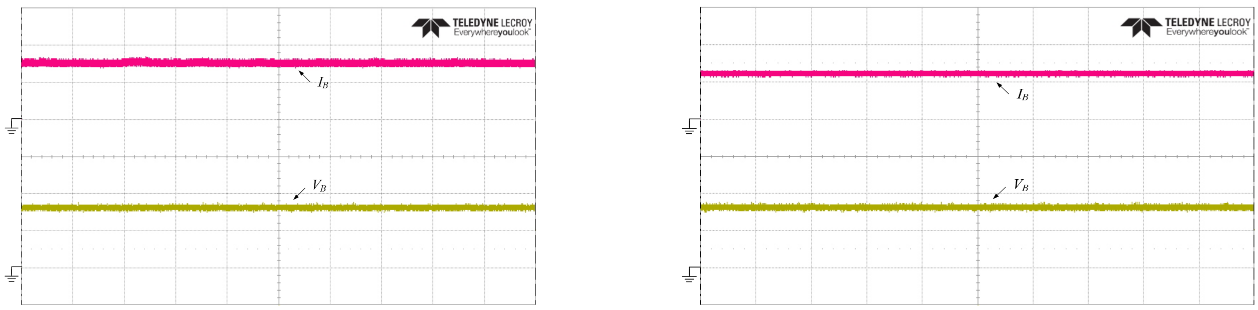

(**a**) (I_B: 2 A/div, V_B: 5 V/div, time: 10 ms/div) (**b**) (I_B: 5 A/div, V_B: 5 V/div/div, time: 10 ms/div)

Figure 16. Measured battery voltage V_B and current I_B waveforms: (**a**) under I_B = 3 A and (**b**) under I_B = 6 A when V_{PV} = 36 V.

When the proposed hybrid converter uses solar power as its input source, it has to possess a good dynamic response. In order to verify the dynamic response of the proposed hybrid converter, Figure 17 illustrates measured battery voltage V_B and current I_B waveforms under step-load changes between I_B = 0 A and $I_{B(max)}$ = 12 A. In Figure 17, battery voltage V_B varies within ±1%, from which it can be observed that the proposed hybrid converter operated in the solar power condition has a good dynamic response. Figure 18 shows measured solar power voltage V_{PV}, current I_{PV} and power P_{PV} waveforms under the maximum solar power $P_{PV(max)}$ = 50 W. In Figure 18, when solar power P_{PV} varies from 0 W to 50 W, the MPPT time interval is about 330 ms. That is, the proposed hybrid converter can achieve MPPT features. Figure 19 expresses the conversion efficiency curve of the proposed hybrid converter operated in the solar power condition from light load to heavy load. In Figure 19, the maximum conversion efficiency is 95% under 80% of the full-load condition. When the proposed hybrid converter is operated under 100% of full-load condition, its conversion efficiency is about 91%. According to power loss analysis, driving circuit and stray losses are about 21.7% of total power loss. Losses of switches are approximated to 42.7%, while losses of transformer T_r are approximately 35.6%. As mentioned above, the proposed hybrid converter can be operated in the solar power condition to achieve battery charging.

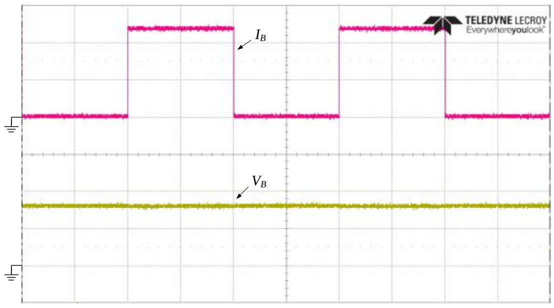

(I_B: 5 A/div, V_B: 5 V/div/div, time: 50 ms/div)

Figure 17. Measured battery voltage V_B and current I_B waveforms under step-load changes between I_B = 0A and $I_{B(max)}$ = 12A when battery voltage V_B = 8V.

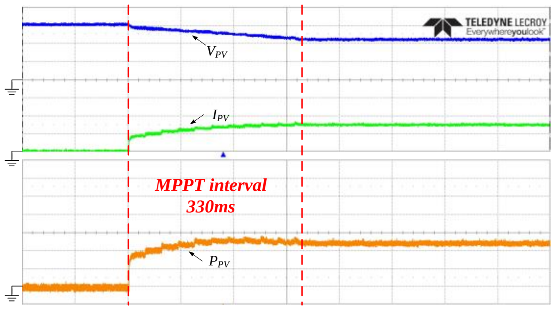

(V_{PV}: 15 V/div/div, I_{PV}: 1 A/div, P_{PV}: 20

Figure 18. Measured solar voltage V_{PV}, current I_{PV} and power P_{PV} waveforms under the maximum solar power $P_{PV(max)}$ = 50W.

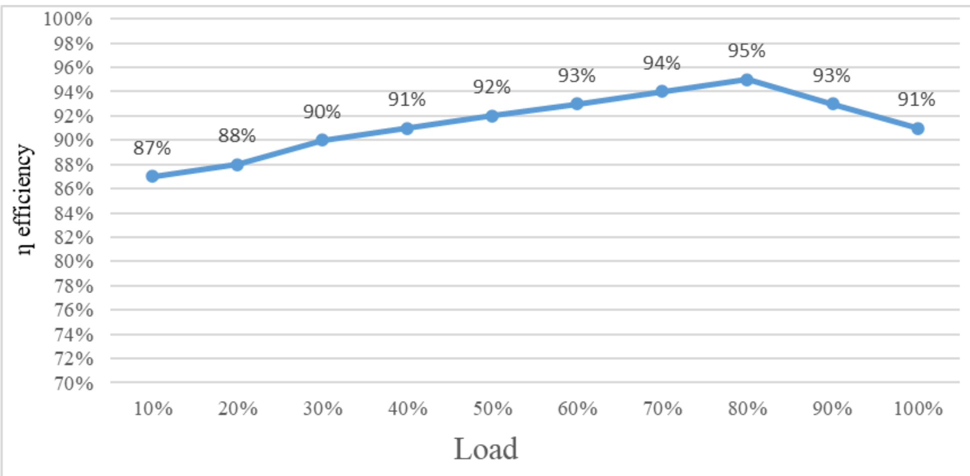

Figure 19. Conversion efficiency curve of the proposed hybrid converter operated in the solar power condition from light loads to heavy loads.

When the proposed hybrid converter adopts the utility line as its input source, some experimental results are measured to verify its feasibility. Figures 20 and 21 illustrate measured switch voltage V_{DS} and current I_{DS} of the proposed hybrid converter operated in the utility line condition. Figure 20 shows those waveforms under 45% of the full-load condition, while Figure 21 expresses those waveforms under 100% of the full-load condition. From Figures 20 and 21, it can be observed that switches M_1 and M_2 are operated with ZVS at the turn-on transition. Figure 22 depicts measured battery voltage V_B and current I_B waveforms of the proposed one operated in the utility line condition under different charging currents. Figure 22a shows those waveforms under I_B = 3 A, while Figure 22b illustrates those waveforms under I_B = 6 A. In Figure 22, the charging current I_B can be successfully changed. Measured battery voltage V_B and current I_B waveforms of the proposed one operated in the utility line condition under step-load changes from I_B = 2.4 A to $I_{B(max)}$ = 12 A are illustrated in Figure 23. Its battery voltage, V_B, can be kept within ±1% to verify a good dynamic response. Figure 24 draws the conversion efficiency curve of the proposed one operated in the utility line condition from light loads to heavy loads. The maximum conversion efficiency is about 93% under 70% of the full-load condition. When the proposed hybrid converter is operated under 100% of the full-load condition, its conversion efficiency is about 89%. According to power loss analysis, driving circuit and stray losses is about 4.3% of total power loss. Losses of switches are approximated to 88.1%, while losses of transformer T_r are approximately 7.6%. As previously experiment results, the proposed hybrid converter can be operated in the utility line condition to achieve battery charging.

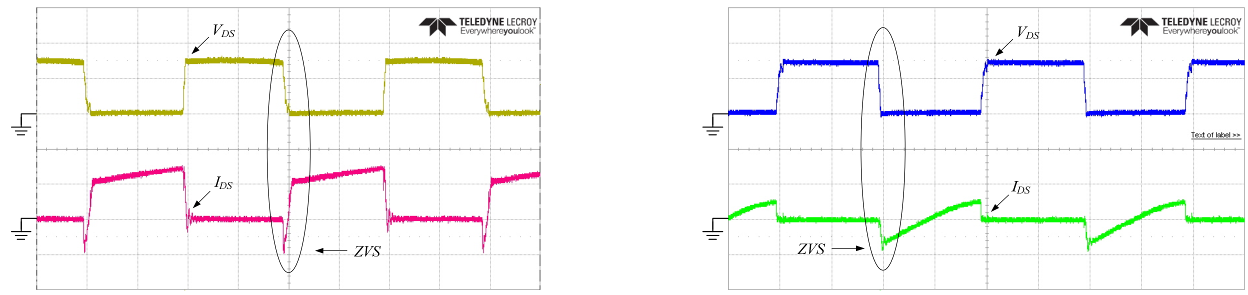

(**a**) (V_{DS}: 200 V/div, I_{DS}: 1 A/div, time: 5 µs/div) (**b**) (V_{DS}: 200 V/div, I_{DS}: 2 A/div, time: 5 µs/div)

Figure 20. Measured switch voltage V_{DS} and current I_{DS} of the proposed hybrid converter operated in the utility line condition under 45% of the full-load condition: (**a**) switch M_1 and (**b**) switch M_2.

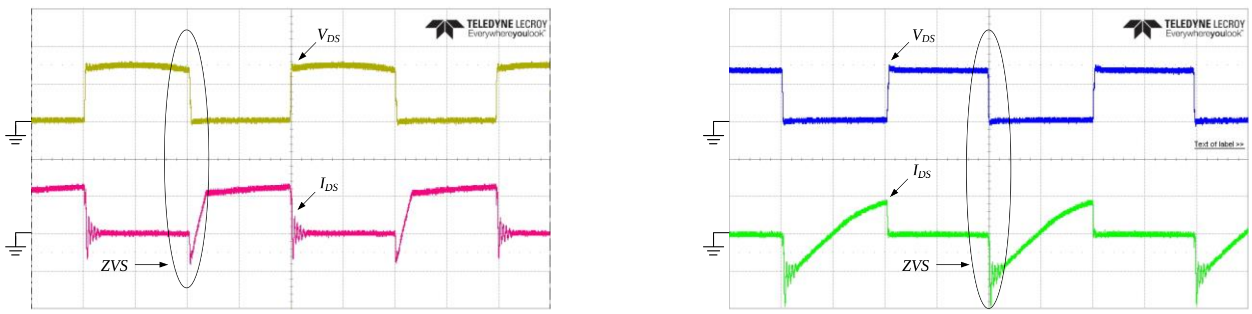

(**a**) (V_{DS}: 200 V/div, I_{DS}: 2 A/div, time: 5 µs/div) (**b**) (V_{DS}: 200 V/div, I_{DS}: 2 A/div, time: 5 µs/div)

Figure 21. Measured switch voltage V_{DS} and current I_{DS} of the proposed hybrid converter operated in the utility line condition under 100% of the full-load condition: (**a**) switch M_1 and (**b**) switch M_2.

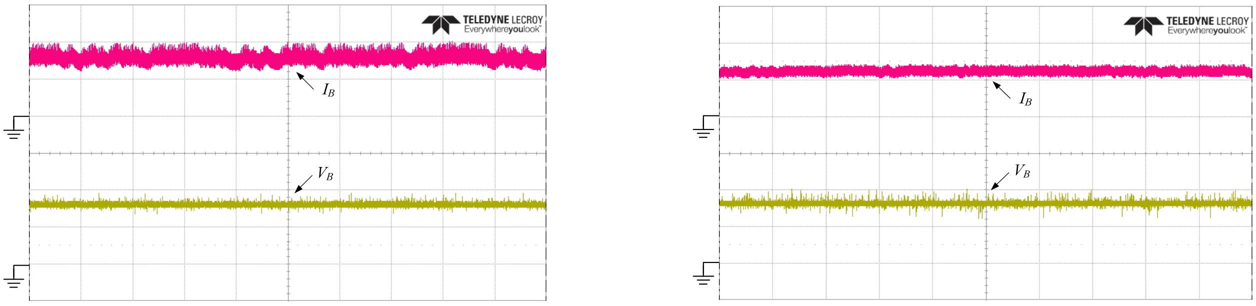

(**a**) (I_B: 2 A/div, V_B: 5 V/div, time: 10 ms/div) (**b**) (I_B: 5 A/div, V_B: 5 V/div/div, time: 10 ms/div)

Figure 22. Measured battery voltage V_B and current I_B waveforms of the proposed hybrid converter operated in the utility line condition (**a**) under I_B = 3 A and (**b**) under I_B = 6 A.

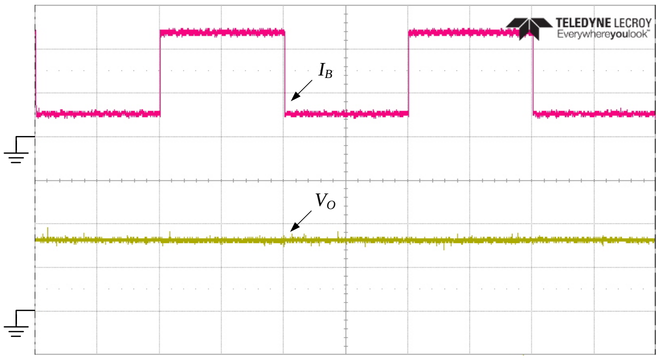

(I_O: 5 A/div, V_O: 5 V/div/div, time: 50 ms/div)

Figure 23. Measured battery voltage V_B and current I_B waveforms of the proposed hybrid converter operated in the utility line condition under step-load changes from I_B = 2.4A to $I_{B(max)}$ = 12A.

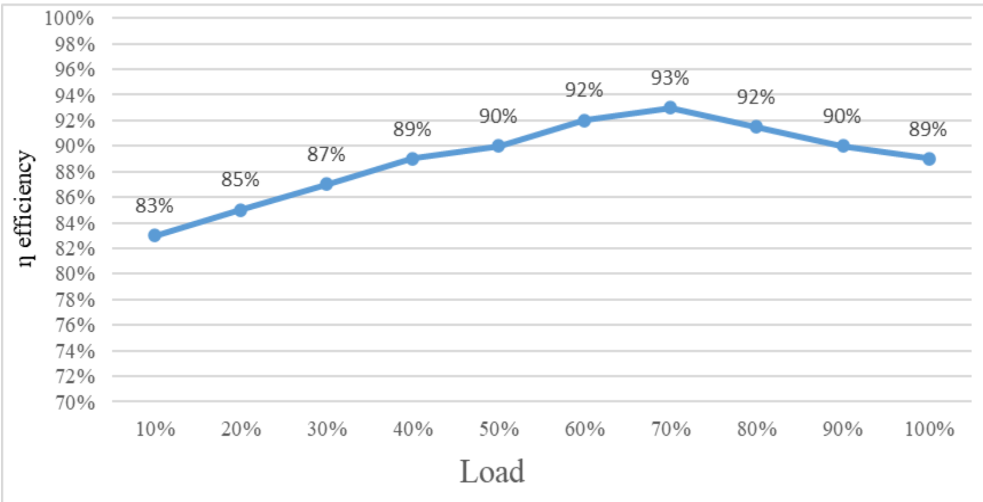

Figure 24. Conversion efficiency curve of the proposed hybrid converter operated in the utility line condition from light loads to heavy loads.

7. Conclusions

This paper proposes a hybrid converter using multiple sources to charge lithium battery. The proposed hybrid converter consists of a buck converter and flyback converter to achieve battery charging under different input sources. Compared with its counterparts, the proposed hybrid converter can reduce component counts when the proposed one adds an extra switch with low speed and low cost. In this paper, circuit simplification of the proposed one is described for reducing component counts. In addition, operational principles, steady-state analysis and design of the proposed converter have been described in detail. From experiment results, it can be observed that the proposed hybrid converter can be operated in different input sources, such as the utility line and solar power sources. When the proposed hybrid converter is operated in the solar power condition, it can implement different charging currents and achieve MPPT operations. Moreover, its maximum conversion efficiency is about 95% under 80% of the full-load condition and its conversion efficiency of the full-load condition is about 91%. When the proposed one is operated in the utility line condition, switches M_1 and M_2 can be operated with ZVS at the turn-on transition. Its maximum conversion efficiency is about 93% under 70% of the full-load condition, and its conversion efficiency of the full-load condition is about 89%. An experimental prototype has been implemented for lithium battery charger of 8.4 V/12 A. It can verify the feasibility of the proposed hybrid converter for lithium battery charging under different input sources.

Author Contributions: Conceptualization, S.-Y.T.; Formal analysis, J.-H.F.; Validation, H.-K.H. All authors have read and agreed to the published version of the manuscript.

Funding: This research was funded by MOST in Taiwan, grant number MOST 110-2221-E-182-040.

Conflicts of Interest: The authors declare no conflict of interest.

References

1. Veeramallu, V.K.S.; Porpandiselvi, S.; Narasimharaju, B.L. A Nonisolated Wide Input Series Resonant Converter for Automotive LED Lighting System. *IEEE Trans. Power Electron.* **2021**, *36*, 5686–5689. [CrossRef]
2. Malschitzky, A.; Agostini, E.; Nascimento, C.B. Integrated Bridgeless-Boost Nonresonant Half-Bridge Converter Employing Hybrid Modulation Strategy for LED Driver Applications. *IEEE Trans. Ind. Electron.* **2021**, *68*, 8049–8060. [CrossRef]
3. Cao, Y.; Li, K.; Lu, M. Balancing Method Based on Flyback Converter for Series-Connected Cells. *IEEE Access* **2021**, *9*, 52393–52403. [CrossRef]
4. Singh, B.; Kushwaha, R. Power Factor Preregulation in Interleaved Luo Converter-Fed Electric Vehicle Battery Charger. *IEEE Trans. Ind. Appl.* **2019**, *57*, 2870–2872. [CrossRef]
5. Abdelmessih, G.Z.; Alonso, J.M.; Tsai, W.T. Analysis and Experimentation on a New High Power Factor Off-Line LED Driver Based on Interleaved Integrated Buck Flyback Converter. *IEEE Trans. Ind. Appl.* **2019**, *55*, 4359–4459. [CrossRef]
6. Abdelmessih, G.Z.; Alonso, J.M. Loss analysis for efficiency improvement of the integrated buck-flyback converter for LED driving applications. *IEEE Ind. Appl. Soc. Annu. Meet.* **2018**, *54*, 6543–6553.
7. Nazi, H.; Babaei, E. A Modularized Bidirectional Charge Equalizer for Series Connected Cell Strings. *IEEE Trans. Ind. Electron.* **2021**, *68*, 6739–6749. [CrossRef]
8. Ahmadi, F.; Adib, E.; Azari, M. Soft Switching Bidirectional Converter for Reflex Charger with Minimum Switches. *IEEE Trans. Ind. Electron.* **2020**, *67*, 8355–8362. [CrossRef]
9. Su, M.; Wu, S.; Dan, H.; Xu, J.; Sun, Y.; Wang, H.; Liu, Y.; Xiong, W.; Liang, X. A Natural Bidirectional Isolated Single-Phase AC/DC Converter with Wide Output Voltage Range for Aging Test Application in Electric Vehicle. *IEEE J. Emerg. Sel. Top. Power Electronics.* **2021**, *9*, 3489–3500. [CrossRef]
10. Hunter, B.L.; Matthews, W.E. A 100-V Battery Charger Voltage Extender IC With 97% Efficiency at 4-A and ±0.5% Voltage Accuracy. *IEEE Trans. Circuits Syst.* **2020**, *67*, 2492–2502. [CrossRef]
11. Wang, C.; Sun, D.; Zhang, X.; Hu, J.; Gu, W.; Gui, S. A Constant Current Digital Control Method for Primary-Side Regulation Active-Clamp Flyback Converter. *IEEE Trans. Power Electron.* **2019**, *36*, 3989–4000.
12. Xu, S.; Qian, Q.; Tao, T.; Lu, S.; Sun, W. Small Signal Modeling and Control Loop Design of Critical Conduction Mode Active Clamp Flyback Converter. *IEEE Trans. Power Electron.* **2019**, *36*, 7250–7263. [CrossRef]
13. Jo, S.W.; Seok, H.; Kim, M. Dual-Mode Resonant Flyback Single Power-Conversion Inverter. *IEEE Trans. Ind. Electron.* **2021**, *68*, 5776–5787. [CrossRef]
14. Jeong, M.G.; Kim, S.H.; Yoo, C. Switching Battery Charger Integrated Circuit for Mobile Devices in a 130-nm BCDMOS Process. *IEEE Trans. Power Electron.* **2016**, *31*, 7943–7952. [CrossRef]
15. Lee, W.S.; Kim, J.H.; Lee, J.Y.; Lee, I.O. Design of an Isolated DC/DC Topology with High Efficiency of over 97% for EV Fast Chargers. *IEEE Trans. Veh. Technol.* **2019**, *68*, 11725–11737. [CrossRef]
16. Aamir, M.; Mekhilef, S. An Online Transformer less Uninterruptible Power Supply (UPS) System with a Smaller Battery Bank for Low-Power Applications. *IEEE Trans. Power Electron.* **2016**, *32*, 233–247. [CrossRef]
17. Mukhtar, N.M.; Lu, D.D.C. A Bidirectional Two-Switch Flyback Converter with Cross-Coupled LCD Snubbers for Minimizing Circulating Current. *IEEE Trans. Ind. Electron.* **2019**, *66*, 5948–5957. [CrossRef]

18. Cheng, H.L.; Chang, Y.N.; Yen, H.C.; Hua, C.C.; Su, S.P. An Interleaved Flyback-Typed LED Driver with ZVS and Energy Recovery of Leakage Inductance. *IEEE Trans. Power Electron.* **2019**, *34*, 4497–4508. [CrossRef]
19. Zhang, F.; Xie, Y.; Hu, Y.; Chen, G.; Wang, X. A Hybrid Boost–Flyback Flyback Microinverter for Photovoltaic Applications. *IEEE Trans. Ind. Electron.* **2020**, *67*, 308–318. [CrossRef]
20. Tseng, S.Y.; Hauang, P.J.; Wu, D.H. Power Factor Corrector with Bridgeless Flyback Converter for DC Loads Applications. *Energies* **2018**, *11*, 3096. [CrossRef]
21. Falcones, S.; Ayyanar, R.; Mao, X. A DC–DC Multiport-Converter-Based Solid-State Transformer Integrating Distributed Generation and Storage. *IEEE Trans. Power Electron.* **2013**, *28*, 2192–2203. [CrossRef]
22. Akar, F.; Tavlasoglu, Y.; Ugur, E.; Vural, B.; Aksoy, I. A Bidirectional Nonisolated Multi-Input DC–DC Converter for Hybrid Energy Storage Systems in Electric Vehicles. *IEEE Trans. Veh. Technol.* **2016**, *65*, 7944–7955. [CrossRef]
23. Kumar, M.; Babu, Y.N.; Pullaguram, D.; Mishra, S. A high voltage gain non-isolated modified three-port DC/DC converter based on integrated Boost-Cuk topology. In Proceedings of the 2017 IEEE PES Asia-Pacific Power and Energy Engineering Conference (APPEEC)s, Bangalore, India, 8–10 November 2017.
24. Wu, H.; Xing, Y.; Xia, Y.; Sun, K. A family of non-isolated three-port converters for stand-alone renewable power system. In Proceedings of the IECON 2011–37th Annual Conference of the IEEE Industrial Electronics Society, Melbourne, Australia, 7–10 November 2011.
25. Wu, H.; Zhang, J.; Xing, Y. A Family of Multiport Buck–Boost Converters Based on DC-Link-Inductors (DLIs). *IEEE Trans. Power Electron.* **2015**, *30*, 735–746. [CrossRef]
26. Wu, Y.E.; Chiu, P.N. A High-Efficiency Isolated-Type Three-Port Bidirectional DC/DC Converter for Photovoltaic Systems. *Energies* **2017**, *10*, 434. [CrossRef]
27. Manoharan, P.; Subramaniam, U.; Babu, T.S.; Padmanaban, S.; Bo, J.; Nielsen, H.; Mitolo, M.; Ravichandran, S. Improved Perturb and Observation Maximum Power Point Tracking Technique for Solar Photovoltaic Power Generation Systems. *IEEE Syst. J.* **2021**, *15*, 3024–3035. [CrossRef]